Microplane Model M5 with Kinematic and Static Constraints for Concrete Fracture and Anelasticity. I: Theory

Zdeněk P. Bažant, F.ASCE,[1] and Ferhun C. Caner[2]

Abstract: Presented is a new microplane model for concrete, labeled M5, which improves the representation of tensile cohesive fracture by eliminating spurious excessive lateral strains and stress locking for far postpeak tensile strains. To achieve improvement, a kinematically constrained microplane system simulating hardening nonlinear behavior (nearly identical to previous Model M4 stripped of tensile softening) is coupled in series with a statically constrained microplane system simulating solely the cohesive tensile fracture. This coupling is made possible by developing a new iterative algorithm and by proving the conditions of its convergence. The special aspect of this algorithm (contrasting with the classical return mapping algorithm for hardening plasticity) is that the cohesive softening stiffness matrix (which is not positive definite) is used as the predictor and the hardening stiffness matrix as the corrector. The softening cohesive stiffness for fracturing is related to the fracture energy of concrete and the effective crack spacing. The postpeak softening slopes on the microplanes can be adjusted according to the element size in the sense of the crack band model. Finally, an incremental thermodynamic potential for the coupling of statically and kinematically constrained microplane systems is formulated. The data fitting and experimental calibration for tensile strain softening are relegated to a subsequent paper in this issue, while all the nonlinear triaxial response in compression remains the same as for Model M4.

DOI: 10.1061/(ASCE)0733-9399(2005)131:1(31)

CE Database subject headings: Concrete; Fracture; Inelastic action; Damage; Softening; Finite element method; Numerical models.

Introduction, Background, and Objective

Except for the growth of spherical voids and collapse of spherical pores, which is not typical of concrete, almost all of the inelastic deformations in concrete microstructure, such as slip, friction, tensile microcrack opening, axial splitting, and lateral spreading in compression, occur on well defined planes taking any spatial orientation. Although these deformations occur at different points in the microstructure, the microplane models concentrate all such deformations, occurring in a small representative volume of the microheterogeneous material, into one point of the macroscopic smoothing continuum. Thus the constitutive properties characterizing these oriented inelastic phenomena (as well as the spherical voids and pores, if any) can be described by means of stress and strain vectors acting on a plane of arbitrary spatial orientation, called the microplane (Bažant 1984). The microplanes may be imagined as the tangent planes of an elemental sphere surrounding every continuum point [Fig. 1].

The strain and stress vectors on the microplanes, $\mathbf{e}$ and $\boldsymbol{\sigma}$, must be assumed to be constrained in some way to the strain and stress tensors of the macrocontinuum, e_{ij} and σ_{ij} (the indices refer to components in Cartesian coordinates $x_i, i=1, 2, 3$). The constraint is said to be kinematic (or static) if the strain (or stress) vector on each microplane is the projection of the continuum strain (or stress) tensor, i.e., $(\mathbf{e})_j = n_i e_{ij}$ and $(\boldsymbol{\sigma})_j = n_i \sigma_{ij}$ (where n_i is the unit normal vector of the microplane). The stresses (or strains) in a kinematically (or statically) constrained microplane model cannot be the stress tensor projections but are related to the $\mathbf{e}$ (or $\boldsymbol{\sigma}$) only by a weak variational constraint, represented by the principle of virtual work (or complementary virtual work). The condition of tensorial invariance is automatically satisfied by considering planes of all orientations.

Compared to the classical tensorial constitutive models based on tensorial invariants, the microplane concept has potent advantages: (1) As realized already by Taylor (1938), a constitutive law in terms of vectors rather than tensors is clearer, conceptually simpler, and easier to formulate. (2) The vector representation can directly characterize the aforementioned oriented deformations as well as their localization into one preferred orientation (note for example that, by contrast, a relationship between the hydrostatic pressure and the second deviatoric stress invariant cannot describe frictional slip on a plane of a specific orientation). (3) The so-called vertex effect, an essential characteristic of concrete (Caner et al. 2002) which is generally missed by the classical tensorial models, is exhibited automatically. (4) Apparent deviations from normality in the sense of tensorial plastic models are automatic, since a microplane model for plasticity is equivalent to a large number of simultaneously active yield surfaces, for each of which the normality rule can be satisfied. (5) The constraint of the microplanes automatically provides all the cross effects such as the shear dilatancy and pressure sensitivity. (6) Combinations

[1]McCormick School Professor and W.P. Murphy Professor of Civil Engineering and Materials Science, Northwestern Univ., 2145 Sheridan Rd., Tech A135, Evanston, IL 60208. E-mail: z-bazant@northwestern.edu

[2]Ramón y Cajal Fellow, ETSECCPB-ETCG, Univ. Politecnica de Catalunya, Jordi Girona 1-3, Ed.D2 D.305, Barcelona 08034, Spain. E-mail: ferhun.caner@upc.es; formerly, Visiting Scholar, Northwestern Univ., 2145 Sheridan Rd., Evanston, IL 60208.

Note. Associate Editor: Franz-Josef Ulm. Discussion open until June 1, 2005. Separate discussions must be submitted for individual papers. To extend the closing date by one month, a written request must be filed with the ASCE Managing Editor. The manuscript for this paper was submitted for review and possible publication on January 27, 2003; approved on February 13, 2004. This paper is part of the ***Journal of Engineering Mechanics***, Vol. 131, No. 1, January 1, 2005. ©ASCE, ISSN 0733-9399/2005/1-31–40/$25.00.

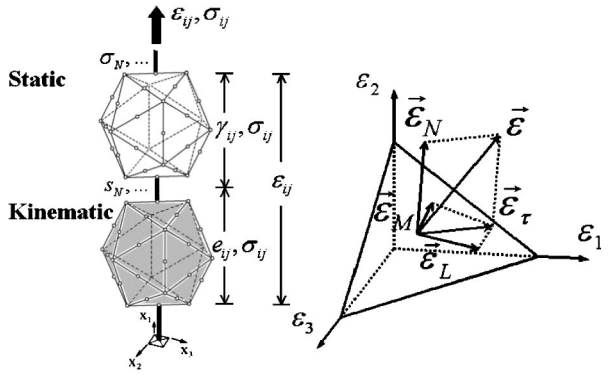

Fig. 1. Left: Coupling of kinematically and statically constrained microplane systems for hardening and softening responses. Right: components of strain or stress vectors on microplane.

of loading and unloading on different microplanes provide a complex path dependence and automatically reproduce the Bauschinger effect and hysteresis under cyclic loading. (7) The dependence of the current yield limits on the strain components (rather than scalar hardening-softening parameters) is easy to take into account. (8) In cyclic loading, fatigue is automatically simulated by accumulation of residual stresses on the microplanes after each load cycle. (9) Finally, anisotropy, while not requisite for concrete, can be captured easily, simply by making the constitutive properties of a microplane dependent on its orientation (in more detail, see Caner and Bažant 2000). These advantages outweigh the burden of a greater amount of computations, a burden that has been waning from year to year with the relentless advance in computer power.

Since its inception (Bažant and Oh 1983a,b, 1985), the microplane constitutive model for concrete has developed into a powerful and robust computational tool for three-dimensional finite element analysis of concrete structures. Initially formulated for concrete as an extension and modification of a groundbreaking idea of Taylor (1938), the evolution of the model has advanced through several progressively improved versions, which were labeled as M1, M2, M3, and M4 for concrete (as described in Bažant et al. 2000a) and M4R for rock (Bažant and Zi 2003). The evolution then ramified to other complex materials such as sand, clay, rigid foam, shape-memory alloys, and fiber composites (Brocca and Bažant 2000, 2001a,b; Brocca et al. 2001). The model was extended to finite strain (Bažant et al. 2000a) and to the rate effect or creep (Bažant et al. 2000c), and has been used in dynamic finite element analyses with up to several million finite elements (Bažant et al. 2000b). Recently, Model M4f (see Part II) introduced into Model M4 a fracture energy based recalibration of softening boundaries in the sense of the crack band theory. The latest version, Model M4 (Bažant et al. 2000a; Caner and Bažant 2000) or M4f describes satisfactorily all the experimentally documented nonlinear triaxial behavior of concrete under compression and shear, and also simulates well the distributed tensile cracking that occurs for strains in the prepeak, peak, and early postpeak regimes.

Problems have nevertheless arisen in predicting the far postpeak tensile response in which the tensile stress across cracks is getting reduced to zero. The objective of this paper is to overcome these problems by formulating a new microplane model, labeled M5. The new model enhances Models M4 and M4f with a statically constrained system of microcracks directly simulating the softening stress-separation law of cohesive fracture (Barenblatt 1959; Rice 1968; Hillerborg et al. 1976; Petersson 1981; Hillerborg 1985; RILEM 1985; Bažant and Planas 1998) or crack band theory (Bažant and Oh 1983a;b).

Need for a Mixed Static-Kinematic Constraint

Although the behavior for strains in the far post-peak tail of the stress–strain diagram is normally irrelevant for predicting the load capacities of structures, it is very important for dynamic response, especially for correctly assessing the energy absorption capability. For the far postpeak tensile strains and for the formation of complete fractures in which the crack bridging stresses are reduced to zero, Model M4, unfortunately, does not perform as well as the simple cohesive crack model or the simple classical smeared cracking models. It is plagued by two problems: (1) At far postpeak tensile softening, the lateral contraction in the directions parallel to the cracks is much larger than the Poisson effect in the material between the cracks and must be judged excessive (even though good test data are lacking, due to the difficulty of capturing strain at a random place where the crack band localizes); and (2) the model exhibits the so-called "stress locking;" in other words, a small but finite tensile stress across the crack band is retained even at extremely large tensile strains.

The cause does not lie in the classical problem of spurious localization and mesh sensitivity, which can be readily avoided by either applying a nonlocal operator or by modifying the postpeak constitutive behavior according to the crack band theory (Bažant and Oh 1983a,b; also Bažant and Planas 1998; Jirásek and Bažant 2002). Rather, the cause lies in the necessity of a kinematic constraint for a softening damage model. The kinematic constraint assumes that the strain vectors on the microplanes are the projections of the strain tensor. Because of this hypothesis, the crack opening produces large tensile strains not only in the microplanes nearly parallel to the cracks but also in those which are significantly inclined to the crack. These inclined microplanes produce large lateral contraction and, since they never soften to zero, they contribute a tensile stress across the cracks even if widely opened.

The problem is aggravated by the necessity of a volumetric–deviatoric split (proposed in Bažant and Prat 1988a,b), i.e., the split of each microplane normal strain into its volumetric and deviatoric components. Such a split is inevitable for a realistic representation of nonlinear triaxial behavior in compression and the transition between compression and tension. In particular, the split is necessary to capture the fact that uniaxial compression and weakly confined compression lead to strain softening with a large lateral expansion, whereas the hydrostatic compression (and compression at zero lateral strain) never leads to any strain softening. This is a troublesome but inevitable dichotomy, which is ignored by most tensorial-type nonlinear triaxial constitutive models for concrete and rock. The split causes that, in far postpeak softening, most of the tensile strain concentrates into the deviatoric component which is tensile in the direction normal to the crack but equally large and compressive in directions parallel to the crack. Eliminating the split merely for tension does not help because it destroys the continuity of transition between the tensile and compressive responses, and restricting the magnitude of volumetric strain (by a volumetric boundary) only alleviates but does not avoid the problem

The kinematic constraint, when introduced in Bažant (1984) and Bažant and Oh (1983b), represented a cardinal departure from the classical Taylor models for metals and nonsoftening (overconsolidated) soils (Batdorf and Budianski 1949; Budianski

and Wu 1962; Lin and Ito 1965, 1966; Brown 1970; Hill and Rice 1972; Zienkiewicz and Pande 1977; Pande and Sharma 1982; Pande and Xiong 1982; Bronkhorst et al. 1992; Butler and McDowell 1998). In Taylor models, the constraint of the planes called here the microplanes is static, i.e., the stress vector on these planes is assumed to be the projection of the stress tensor. As learned from the first studies of softening in fracturing materials at Northwestern University during the early 1980s, the main reason for replacing at that time the static constraint with a kinematic constraint was to stabilize the system of softening microplanes. If there is no softening, as in plastic metals, the static constraint causes no instability because the strain corresponding to a given stress reduction is uniquely defined by the elastic unloading.

But if there is softening, the static constraint inevitably leads to instability because the microplane strains caused by a given stress reduction are not unique, corresponding to either the softening branch or the unloading branch. The consequence is that all the microcracking strains (unlike plastic strains) suddenly localize, under static constraint, into a single microplane of one orientation only. This makes it impossible to simulate a system of microcracks of many orientations, developing simultaneously in the peak stress region. Later on, in the far postpeak response, the cracking of course does localize into one dominant orientation, and that is why we will strive here to enhance Model M4 with a static constraint.

There is also a secondary, physical, reason for the governing role of the kinematic constraint in the peak stress region. Unlike plastic yielding, happening at constant stress, the average local strain tensor of the material around and between the diffuse microcracks is essentially the same as the strain tensor of the macroscopic smoothing continuum. The formation of small microcracks causes the continuum stress to drop without affecting the strain tensor (the same observation underlies the classical Kachanov-type theory of continuum damage mechanics).

Assuming all the behavior to adhere to a strict kinematic constraint is also arguable from the viewpoint of stiffness bounds. From the theory of composite materials (e.g., Christensen 1979), it is well known that the kinematic constraint, corresponding to Voigt's (1889) parallel coupling model, and the static constraint, corresponding to Reuss' (1929) series coupling model, represent the upper and lower bounds on the material stiffness, which are generally not close to each other. The real behavior is somewhere inbetween. Therefore, a microplane model incorporating a mixture of the kinematic and static constraints should be physically more realistic.

There are further reasons for seeking a way to formulate a hybrid constraint. Just like the strains due to plastic slip on a long slip line, the strains due to the opening of continuous cracks (unlike the strains due to small diffuse microcracks) are additive to the elastic strains of the material inbetween and both happen at the same stress. Consequently, the interaction of the elastic strains with the strains due to large and continuous (or almost continuous) cracks should be described by a series coupling model, and so should the interaction of the strains due to long cracks of different orientations. This means that the microplane system for the interaction of the opening of wide and long cracks should have a static rather than kinematic constraint, and that this system should be coupled in series with the microplane system that simulates nonlinear triaxial behavior and diffuse microcracking in the peak stress region.

A mixture of both constraints was attempted at Northwestern already in the early 1980s but seemed unworkable. It took the form of a series coupling of two microplane systems [Fig. 1], in which the strain tensor ϵ_{ij} was decomposed as

$$\epsilon_{ij} = e_{ij} + \gamma_{ij} \tag{1}$$

where e_{ij}, γ_{ij}=strain tensors for the kinematically and statically constrained (nonsoftening and softening) microplane systems, both subjected to the same stress tensor σ_{ij}. Such a coupling, however, caused the microplane strains and stresses of both systems to become tied by many implicit nonlinear equations. This appeared to pose at that time formidable computational difficulties. To circumvent the problem, an iterative algorithm akin to that used in plastic finite element analysis was tried but was found to diverge because of softening. It was for this reason that the pursuit of series coupling model with hybrid constraints was at that time abandoned. Nevertheless, Carol and Bažant (1995) later demonstrated advantages of a series coupling of fracturing microplane system to an elastic microplane system.

Challenge: How to Achieve Convergence of Softening for Static Constraint?

The iterations in each loading step of plastic finite element analysis commonly employ the return mapping algorithm (Hughes 1984; Simo and Hughes 1998), in which the elastic deformation is used as the predictor and a subsequent return to the current yield surface as the corrector. A special case is the radial return algorithm for the J_2 flow theory of plasticity (Wilkins 1964; Krieg and Key 1976; Krieg and Krieg 1977; Simo and Taylor 1985). In these algorithms, the corrector has in fact an infinite negative stiffness since the drop of stress point to the yield surface in the stress space is carried out at constant strain. A direct application of this kind of algorithm to the series coupling of two microplane systems [Fig. 1] is not a feasible approach because a return at constant strain would require solving a system of many nonlinear equations.

To emulate at least the spirit of this algorithm for the series coupling model [Fig. 1], it would seem natural to use the kinematically constrained microplane system with a positive incremental stiffness [Fig. 1, left] as the predictor, and the fracturing statically constrained microplane system [Fig. 1, right] as the corrector. Such a corrector has a finite negative stiffness, and this stiffness is typically smaller in magnitude than the stiffness of the predictor. Unfortunately, though, the convergence of this analog of the return mapping algorithm breaks down (see Algorithm A in Part II).

To achieve convergence, a new kind of iterative algorithm will be introduced. When the statically constrained microplane system [Fig. 1, left] is active (i.e., when cracks are opening), its negative (or negative definite) incremental stiffness will be employed as the predictor, and the positive (or positive definite) stiffness of the kinematically constrained microplane system [Fig. 1, right] will be employed as the corrector. Such an iterative algorithm converges, and does so in a geometric progression, as proven in a later section (Algorithm B or B′). Adopting the softening inelastic part of response as the predictor is the opposite of the algorithms established in computational plasticity, and the reason that this works is that the negative stiffness of the inelastic corrector is not too large in magnitude. An acceleration giving quadratic convergence can further be obtained by using the Newton-Raphson method to subdivide the strain between the two microplane systems.

Review of Basic Relations for Microplane Systems

The microplane system with strain tensor γ_{ij} [Fig. 1] is constrained statically and describes only the strain softening due to the opening of cohesive cracks of various possible orientations. The microplane system with strain tensor $e_{ij}=\epsilon_{ij}-\gamma_{ij}$ is constrained kinematically and describes the elastic deformations and all the remaining inelastic deformations, which exclude cohesive crack softening (but include deviatoric softening needed to simulate the softening in uniaxial compression). According to these constraints

$$e_N = N_{ij}e_{ij}$$

$$e_M = M_{ij}\sigma_{ij} \tag{2}$$

$$e_L = L_{ij}e_{ij}$$

$$\sigma_N = N_{ij}\sigma_{ij}$$

$$\sigma_M = M_{ij}\sigma_{ij} \tag{3}$$

$$\sigma_L = L_{ij}\sigma_{ij}$$

in which $N_{ij}=n_in_j$; $M_{ij}=(m_in_j+m_jn_i)/2$; $L_{ij}=(l_in_j+l_jn_i)/2$; and subscripts M and N label two suitably chosen coordinate directions given by orthogonal unit coordinate vectors of components m_i and l_i, lying in the microplane [Fig. 1]. Microplane strain e_N is further split into its volumetric and deviatoric components

$$e_D = e_N - e_V$$

$$e_V = \tfrac{1}{3}e_{kk} \tag{4}$$

For strains e_N, e_V, e_D, e_M, and e_L, the microplane constitutive law for the kinematically constrained system gives the corresponding stresses s_N, s_V, s_D, s_M, and s_L (which are not the same as the stresses σ_N, σ_V, σ_D, σ_M, and σ_L in the statically constrained part, except by chance). According to the principle of virtual work (Bažant et al. 2000a)

$$\sigma_{ij} = s_V\delta_{ij} + s_{ij}^D$$

$$s_{ij}^D = \frac{3}{2\pi}\int_\Omega s_{ij}\,d\Omega \tag{5}$$

with

$$s_{ij} = s_D\left(N_{ij} - \frac{\delta_{ij}}{3}\right) + s_LL_{ij} + s_MM_{ij}$$

where Ω=surface of a unit hemisphere (in detail, see Bažant et al. 2000a). This integral is evaluated numerically using an optimal Gaussian quadrature formula for a spherical surface (Bažant and Oh 1985, 1986) which represents a weighted sum over the stresses on N_m microplanes with discretely distributed orientations $\mu=1,2,\ldots N_m$;

$$\sigma_{ij} \approx 6\sum_{\mu=1}^{N_m} w_\mu s_{ij}^{(\mu)} + s_V\delta_{ij} \tag{6}$$

where w_μ=quadrature weights ($\Sigma_{\mu=1}^{N_m}=1$).

For the statically constrained microplane system, no volumetric–deviatoric split is introduced. According to the principle of complementary virtual work

$$\gamma_{ij} = \frac{3}{2\pi}\int_\Omega u_{ij}\,d\Omega \tag{7}$$

with

$$u_{ij} = \gamma_NN_{ij} + \gamma_LL_{ij} + \gamma_MM_{ij}$$

In numerical calculations

$$\gamma_{ij} = \frac{3}{2\pi}\int_\Omega u_{ij}\,d\Omega \approx 6\sum_{\mu=1}^{N_m} w_\mu u_{ij}^{(\mu)} \tag{8}$$

A quadrature formula with $N_m=37$ microplanes per hemisphere (Stroud 1971) has been used in the present calculations. Bažant and Oh (1986) studied the accuracy of various formulas in different situations and developed a new, more efficient (albeit less accurate), formula with 21 integration points. [see Fig. 1 where the circular points placed on an icosahedron define the directions of microplane normals.]

Microplane Constitutive Relations of Model M5

The inelastic constitutive laws on the microplanes are defined by the so-called stress–strain boundaries (or strain-dependent softening yield limits, introduced in Bažant et al. 1996a,b). For e_{ij}, these laws are nearly the same as in M4, with minor differences to be described later. Within the boundaries, the incremental response is elastic (like in M4) and described as $\dot{s}_V=E_V\dot{e}_V, \dot{s}_D=E_D\dot{e}_D, \dot{s}_M=E_T\dot{s}_M, \dot{s}_L=E_T\dot{s}_L$, where the superior dots denote the time rates and E_V, E_D, E_T=microplane elastic moduli, the relationship of which to the Young's modulus E and Poisson ratio ν is best taken as $E_V=E/(1-2\nu)$, $E_D=E/(1+\nu)$] and $E_T=E_D$ (as justified in Bažant and Prat 1988a; Carol et al. 1991; Carol and Bažant 1997). Although, upon reaching a boundary curve, the microplane stress–strain curve has a sharp sudden change of slope, the resulting macrocontinuum stress–strain curve is quite smooth because the transitions to the boundary curve happen on different microplanes at different times.

Cohesive Fracture in Tension and Shear

We will assume that a cohesive crack can develop in the direction of any microplane if the tensile strength is exhausted. The relative normal and shear displacements across the crack, δ_N, δ_L, and δ_M, are modeled by normal and shear strains on the microplane

$$\gamma_N = \delta_N/h$$

$$\gamma_L = \delta_L/h \tag{9}$$

$$\gamma_M = \delta_M/h$$

where h=effective width of the band of finite elements representing the fracture (coinciding with the actual size of the elements if the fracture propagates along the mesh line of a square grid). If, however, there is a system of parallel cracks (stabilized for instance by reinforcement or adjacent compressed zone), then h should represent the typical spacing of the parallel cracks. For pure mode (opening) fracture, a cohesive crack is normally characterized by a softening stress-separation function $\sigma_N=\phi(\delta_N)$. We will consider, more generally, a mixed opening-shear cohesive fracture (mixed Modes I, II, and III), for which the vector of cohesive stress $\boldsymbol{\sigma}$ is in general a function of the displacement vector $\boldsymbol{\sigma}$. We will adopt here a recent simplification of Camacho

and Ortiz (1996), which assumes the existence of a potential for the cohesive stresses, $\Psi(\delta)$ (free energy density), where

$$\delta = h\gamma, \tag{10}$$

$$\gamma = \sqrt{\gamma_N^2 + \beta^2(\gamma_L^2 + \gamma_M^2)}$$

Factor β, very small for concrete, expresses the fact that concrete much prefers to fracture in tension than in shear (according to Bažant et al. 1988, the ratio of Mode III to Mode I fracture energies of concrete appears to be about 30, and so $\beta \approx 1/30$). Based on the existence of potential Ψ, $\sigma_N = h^{-1}\partial\Psi/\partial\gamma_N$, $\sigma_L = h^{-1}\partial\Psi/\partial\gamma_L$, and $\sigma_M = h^{-1}\partial\Psi/\partial\gamma_M$. This yields

$$\sigma_N = \gamma_N\sigma/\gamma,$$

$$\sigma_L = \beta^2\gamma_L\sigma/\gamma, \tag{11}$$

$$\sigma_M = \beta^2\gamma_M\sigma/\gamma$$

where

$$\sigma = \sqrt{\sigma_N^2 + (\sigma_L^2 + \sigma_M^2)/\beta^2} \tag{12}$$

The last equation may be verified by substituting Eq. (11). Note that in this model, based on a potential, the cohesive stress vector is always parallel to the stress displacement vector (or to the fracture strain vector) because $\sigma_N/\sigma = \gamma_N/\gamma$, etc. It must be admitted that this property is not realistic in the case of pure shear on the macrocontinuum level, because it implies zero dilatancy. For the shear on a microplane, however, this is not a problem since dilatancy is automatically created by the interaction of microplanes of different orientations, simply as a result of the fact that the strength is lower in tension than in compression (Bažant and Gambarova 1984; Bažant et al. 2000a).

During the initial elastic and inelastic stress increase, the cracks remain closed and so the strains on the statically constrained microplane system remain zero. When the microplane normal stress σ_N reaches the strength limit f_t' in tension, a coplanar cohesive crack is assumed to form on that microplane. σ_N is imagined to represent the cohesive (crack-bridging) stress transmitted between the faces of this crack, which is determined by the softening law $\sigma_N = f(w)$ where w is the separation between the crack faces (crack opening); w can be related to the fracturing part of the total strain by $\gamma_N = w/s$ where s is the effective crack spacing (between parallel cracks of about the same orientation as the microplane). The softening stress-separation relation is assumed to be bilinear.

Furthermore, microplane fracturing compliances on every microplane of the statically constrained system and a fracturing compliance tensor on the macro scale must be defined in order to implement an efficient algorithm for the additive split of the strains. To this end, it is convenient to write the split of the increment of total strain as $f_i = -\Delta e_i - \Delta\gamma_i + \Delta\epsilon_i = 0$ using the convenience of Voigt notation (where $i = 1, 2, \ldots 6$; $\Delta_{e_1}, \ldots \Delta_{e_6}$ correspond to $\Delta_{e_{11}}, \ldots 2\Delta_{e_{31}}$). Fixing $\Delta\epsilon_i$ at a given load step, and using $\Delta\sigma_i = K_{\text{in}}\Delta e_n$ and $\Delta\gamma_i = C_{\text{in}}^f\Delta\sigma_n$ where K_{in} is the elastic 6×6 stiffness matrix and C_{in}^f is the fracturing compliance matrix, the linearized problem becomes $f_i(\Delta e_n^0) + C_{\text{in}}\delta(\Delta e_n) \approx 0$ in which

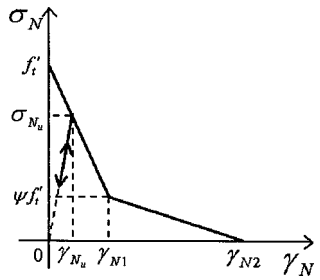

Fig. 2. Bilinear softening relation for normal microplane stresses and strains, and relation for crack unloading and reloading

$$G_{ij} = \frac{\partial f_i}{\partial(\Delta e_j)} = -\frac{\partial(\Delta\gamma_i)}{\partial(\Delta e_j)} - \delta_{ij} = -\frac{\partial(\Delta\gamma_i)}{\partial(\Delta\sigma_n)}\frac{\partial(\Delta\sigma_n)}{\partial(\Delta e_j)} - \delta_{ij} = -C_{\text{in}}^f K_{nj} - \delta_{ij} \tag{13}$$

Here, $C_{\text{in}}^f = \partial(\Delta\gamma_i)/\partial(\Delta\sigma_n)$ can be calculated using Eq. (7) as

$$C_{\text{in}}^f = \frac{3}{2\pi}\int_\Omega \left(\frac{\partial(\Delta\gamma_N)}{\partial(\Delta\sigma_N)}\frac{\partial(\Delta\sigma_N)}{\partial(\Delta\sigma_n)}N_i + \frac{\partial(\Delta\gamma_M)}{\partial(\Delta\sigma_M)}\frac{\partial(\Delta\sigma_M)}{\partial(\Delta\sigma_n)}M_i + \frac{\partial(\Delta\gamma_L)}{\partial(\Delta\sigma_L)}\frac{\partial(\Delta\sigma_L)}{\partial(\Delta\sigma_n)}L_i\right)d\Omega \tag{14}$$

which simplifies to

$$C_{\text{in}}^f = \frac{3}{2\pi}\int_\Omega (C_N^f N_i N_n + C_M^f M_i M_n + C_L^f L_i L_n)d\Omega \tag{15}$$

where $C_N^f = \gamma/\sigma$ is normal compliance and $C_M^f = C_L^f = \beta^{-2}\gamma/\sigma$ = shear fracturing compliances defined on each microplane of the statically constrained microplane system, and C_{in}^f = corresponding compliance tensor.

Fracturing Properties of Statically Constrained Microplanes

The softening response in pure tension or tension combined with shear is expressed by means of the fracturing strain tensor γ_{ij} and is described by the statically constrained microplane system. No elastic response is included in γ_{ij}. Since $\gamma_N = \delta_N/s$ where δ_N = crack opening, the microplane softening law is defined as a scaled softening law for the cohesive crack model. The bilinear softening law (Fig. 2), well justified for concrete fracture (Petersson 1981; Hillerborg 1985; RILEM 1985; Guinea et al. 1994; Bažant and Planas 1998), is adopted:

$$\sigma_N = f_t' \max\left[1 - \frac{1-\psi}{\gamma_{N1}}\gamma_N, \psi\max\left(1 - \frac{\gamma_N - \gamma_{N1}}{\gamma_{N2} - \gamma_{N1}}, 0\right)\right] \tag{16}$$

where $0 \leqslant \psi < 1$ and the points $(0, f_t')$, $(\gamma_{N1}, \psi f_t')$, and $(\gamma_{N2}, 0)$ in the diagram of normal stress versus fracturing strain on the microplane define the bilinear cohesive law (Fig. 2). The foregoing softening law is defined only for $\gamma_N \geqslant 0$ because negative crack opening can never occur.

As soon as the axial response reaches f_t' on one microplane, the crack on that microplane begins to open while all the other microplanes normally begin unloading. Thus the fracture process

normally localizes into one single microplane. As the crack for that microplane continues to open, the normal stress and crack opening displacement sweep the area under the prescribed softening curve. The areas under the entire softening curve $\sigma = f(w)$ and under the initial tangent of this curve represent the Mode I fracture energies

$$G_F = \int_0^{\infty} \sigma_N \, dw = s \int_0^{\gamma_{N2}} \sigma_N d\gamma_N \tag{17}$$

$$G_f = \frac{f_t' \gamma_{N1}}{2(1-\psi)}$$

(the integral for G_F was justified by Rice 1968); G_f=fracture energy that normally governs the maximum loads of notched specimens and structures with large stress-free cracks (Bažant and Planas 1998; Bažant et al., private communication 2002) because the cohesive stress at the notch tip at maximum load is normally not yet reduced to a value less than $\psi f_t'$.

If both G_F and G_f have been measured for the given concrete (Bažant et al., private communication 2002), it suffices to choose a suitable value for ψ and then the softening law is fully defined. Analysis of notched fracture test data gives roughly $\psi \approx 1/4$ (Bažant and Planas 1998); however, van Mier's uniaxial tensile test data are optimally fitted with $\psi \approx 0.44$. As a compromise, all the present data fitting has been done with $\psi = 0.3$, even though it does not yield optimum fits. If only G_F has been measured, one must also choose the ratio G_f/G_F (a suitable choice is 0.4; Bažant and Planas 1998; Bažant and Becq-Giraudon 2002), or the value γ_{N1}. Instead of G_F, one can specify γ_{N2} (a suitable value may be roughly 0.03). Using the tensile strength data for concrete specimens of different sizes, one can determine G_f for the type of concrete used from the size effect law. The values of ψ and γ_{N2} can be assumed to be fixed at certain values for all concretes (e.g., $\psi = 0.44$ and $\gamma_{N2} = 0.03$), and one can thus obtain the approximation $\gamma_{N1} \approx 1.34 G_f (1-\psi)/s f_t'$ where factor 1.34 is obtained for $\psi = 0.44$. Note that if the initial slope of the softening curve is chosen too steep, convergence problems may result.

The unloading and reloading of the cohesive crack are assumed to be linear, as sketched in Fig. 2. They are defined by the relation

$$\gamma_N = \gamma_{N_u}(1 + k_u \Delta\sigma_N / \sigma_{N_u}) \tag{18}$$

where $\Delta\sigma_N < 0$ for unloading; γ_{N_u}=maximum γ_N attained so far (which must be saved, for each microplane); σ_{N_u}=corresponding stress, and k_u=coefficient defining the degree of reversibility of crack opening. For $k_u = 1$ the opening is fully reversible and for $k_u = 0$ it is irreversible. In reality, the opening is partially reversible ($0 < k_u < 1$), because of the microscopic debris deposited between the crack faces and because of irreversibility of the frictional slip in the fracture process zone. For computations, $k_u = 1$ has been assumed. If $k_u < 1$ is chosen, for the sake of simplicity and also due to lack of good test data, the difference between the unloading and reloading paths may be neglected (although it would not be difficult to program it). Note that, regardless of the value of k_u, the unloading is governed by the kinematically constrained part.

Constitutive Properties of Kinematically Constrained Microplanes

For the kinematically constrained microplanes subjected to strain tensor ϵ_{ij}, we try to follow microplane Model M4 for concrete as far as possible. What needs to be removed from Model M4 (Fig. 3) is the softening portions of the stress–strain boundaries for tensile normal strain and tensile volumetric strain on the microplanes because the softening in pure tension and in tension with shear is already represented by the softening cohesive law for the statically constrained microplanes. In consequence, the frictional shear boundary used in M4 needs to be adjusted as well. It is fortunate that the necessary modifications have no effect on the nonlinear triaxial response in compression and shear, and so most of the features of Model M4, tediously calibrated in previous work, can be retained.

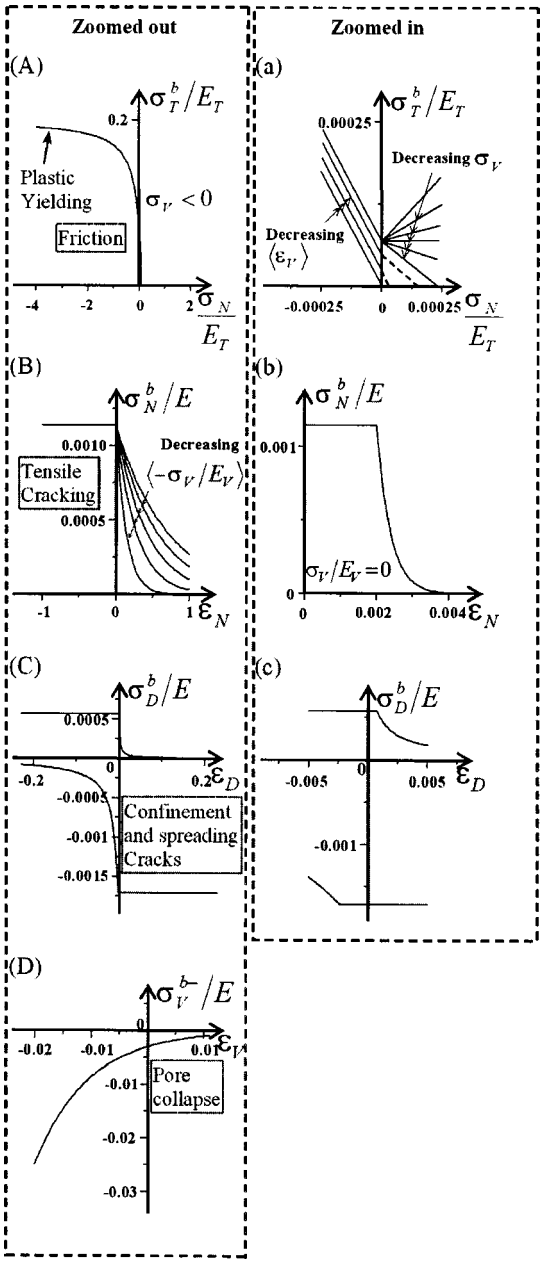

Fig. 3. Stress–strain boundaries of kinematically constrained microplane system, co-opted from Model M4 with modifications

Normal Boundary

The microplane normal boundary (i.e, the boundary on s_N), which in M4 and M4f governs primarily the tensile softening, might seem redundant since the tensile softening is modeled by the stati-

cally constrained microplanes. Not quite, however, since this boundary is also important for the postpeak softening in uniaxial compression. Thus, the normal boundary is kept the same as it is in Model M4 or M4f (Fig. 3), even though it now serves only to restrict excessively large lateral expansion under uniaxial compression. It has no effect on the tensile response in the current model, because the cohesive softening law for the statically constrained microplanes is activated before this normal boundary is approached. Once the softening on the statically constrained microplanes becomes activated, the kinematically constrained microplane system unloads, due to series coupling.

Volumetric Boundary

In Models M4 and M4f, the normal boundary that bounds the normal stress s_N was alone insufficient to prevent volumetric stress s_V from growing too large because the softening effect of the normal boundary was offset by increasing s_V. Therefore, it was necessary to also impose a softening tensile volumetric boundary (Bažant et al. 2000a). In the current model, the problem of growing tensile stress at large ϵ_V never occurs because the volumetric and deviatoric stresses unload while the statically constrained microplanes provide softening in tension. Thus, the series coupling in the present model makes the tensile volumetric boundary in tension superfluous.

Shear Boundary

The shear boundary has different roles in tension and compression. In compression, it serves as a frictional yield surface in the plane of shear stress versus normal stress, with the cohesion gradually approaching zero as the fracturing damage increases. In the tensile range, however, the frictional boundary cannot be closed, as in M4, because it would cause excessive prepeak plastic strain and shift the stress peak too far. Rather, the shear response in tension must remain almost elastic until the peak, which is ensured by elevating the tensile portion of the frictional boundary as shown in Fig. 3. Thus, in tension, the frictional boundary is formulated as a shear stress bound proportional to the tensile normal stress. The modification of the frictional shear boundary of M4 (Fig. 3) is mathematically described as follows:

$$\text{for } s_N > 0$$

$$s_T^b = \langle s_T^0 + c_{22}\epsilon_V^{\text{eq}} s_N \rangle \tag{19}$$

where

$$s_T^0 = c_{10}\frac{s_0}{1 + c_{10}s_0/(k_1k_2E_T)}$$

$$s_0 = \frac{E_T k_1 c_{11}}{1 + c_{12}\langle \epsilon_V/k_1 \rangle} \tag{20}$$

Here, $c_{22}=1\times10^5$ and $c_{12}=0.155$, while all the other parameters have the same values as given in Caner and Bažant (2000).

The shear boundary for compressive s_N is as given in Bažant et al. (2000a,b,c):

$$\text{for } s_N < 0$$

$$s_T^b = \frac{E_T k_1 k_2 c_{10}\langle -s_N + s_N^0 \rangle}{E_T k_1 k_2 + c_{10}\langle -s_N + s_N^0 \rangle} \tag{21}$$

where $\langle X \rangle = \max(X,0)$ = positive part of argument. If $\langle \epsilon_V \rangle$ is large, $c_{10}=[ds_T^b/ds_N]_{s_N=0}$ = initial slope of the boundary, and $\lim_{s_N\to\infty} s_T^b = E_T k_1 k_2$, which represents a horizontal asymptote.

Making the slope a function of ϵ_V^{eq} for tensile s_N makes it possible to distinguish important qualitative differences between compression and tension. For compression, this function causes the slope to be negative and thus the yield surface to be closed. For tension, this slope is positive, thus allowing a linear shear response until the tensile strength is reached on a statically constrained microplane, and in this way the statically constrained microplane system is made to control the tensile softening.

Incremental Thermodynamic Potential

Two kinds of thermodynamic potentials are of interest: (1) the complete potential, which is a function of the reversible parts of total strains and involves separate internal state variables for irreversible strains governing energy dissipation; and (2) the incremental potential associated with the tangential (inelastic) moduli tensor, considered as given and thus equivalent to an elastic moduli tensor. The latter, which does not separate the reversible (elastic) and irreversible (inelastic) deformations, cannot capture energy dissipation but can capture the entropy produced by deviations from equilibrium, which is what is needed to detect bifurcation and identify the actual postbifurcation equilibrium path (as explained in Bažant 1988 and in Section 10.2 of Bažant and Cedolin 1991). Only the latter will be presented here. The former could be obtained if the latter is generalized by separation of reversible and irreversible deformations. This would require extending the analysis of Carol et al. (2001, 2004) from a kinematically constrained to a hybrid microplane model, and is beyond the scope of this paper. Note that the microplane formulation presented does not rest on the incremental potential but is derived from the principles of virtual work and complementary virtual work.

Because of mixing the kinematic and static constraints, an incremental potential representing the specific free energy, of either Helmholtz or Gibbs type, does not exist on the macrocontinuum level (the term "specific" means "per unit volume," and "density" "per unit mass"). Nevertheless, a potential for microplane models with mixed constraints can be defined. From the theoretical and computational viewpoints, this is an attractive aspect, which will now be demonstrated.

The total variation of the specific Helmholtz free energy Ψ of a continuum with a constitutive law described by the microplane Model M5 may be expressed as

$$\rho\Psi = \int_{\Omega'} \Psi_{\mathbf{n}}(\mathbf{e}^n)d\Omega' + \int_{\Omega'} \Phi_{\mathbf{n}}(\gamma^\sigma)d\Omega' \tag{22}$$

$$\delta(\rho\Psi) = \int_{\Omega'} \frac{\partial \Psi_{\mathbf{n}}}{\partial \mathbf{e}^n}\cdot\delta\mathbf{e}^n\,d\Omega' + \int_{\Omega'} \frac{\partial \Phi_{\mathbf{n}}}{\partial \gamma^\sigma}\cdot\delta\gamma^\sigma\,d\Omega'$$

$$= \int_{\Omega'} \mathbf{s}^e\cdot\left(\frac{\partial \mathbf{e}^n}{\partial \mathbf{e}}\cdot\delta\mathbf{e}\right)d\Omega' + \int_{\Omega'} \boldsymbol{\sigma}^n\cdot\delta\gamma^\sigma d\Omega' \tag{23}$$

in which

$$\mathbf{s}^e = \partial\Psi_{\mathbf{n}}/\partial\mathbf{e}^n \tag{24}$$

$$\boldsymbol{\sigma}^n = \partial \Phi_{\mathbf{n}} / \partial \gamma^{\sigma}$$

and $\partial \mathbf{e}^n / \partial \mathbf{e} = \mathbf{n}$. Here $\Omega' = (2\pi/3)\Omega = (2\pi/3)\sin\theta \, d\phi \, d\theta$ (ϕ, θ being spherical coordinates); ρ=mass density; $\Psi_{\mathbf{n}}$ or $\Phi_{\mathbf{n}}$=contributions to the variation of the Helmholtz free energy density from microplane of orientation $\mathbf{n}, \Omega$=surface of a unit hemisphere; $\mathbf{e^n}, \mathbf{s^e}$=strain and stress vectors on kinematically constrained microplane of orientation $\mathbf{n}$, and $\gamma^{\sigma}, \boldsymbol{\sigma}^{\mathbf{n}}$=strain and stress vectors on statically constrained microplane of orientation $\mathbf{n}$ (corresponding to spherical coordinates ϕ, θ, the latitude, and longitude); $\boldsymbol{\sigma}^{\mathbf{e}}$=microplane stress vector corresponding to $\mathbf{e^n}$ in the kinematically constrained part, and γ^{σ}=microplane strain vector corresponding to $\boldsymbol{\sigma}^{\mathbf{n}}$ in the statically constrained part; $\mathbf{e^n} = \mathbf{e} \cdot \mathbf{n}, \boldsymbol{\sigma}^{\mathbf{n}} = \boldsymbol{\sigma} \cdot \mathbf{n}, \boldsymbol{\varepsilon} = \mathbf{e} + \boldsymbol{\gamma}$, where $\boldsymbol{\sigma}, \boldsymbol{\varepsilon}$=macrocontinuum stress and strain tensors; and $\mathbf{e}, \boldsymbol{\gamma}$=partial strain tensors of macrocontinuum corresponding to the kinematically and statically constrained microplane systems.

Substituting the tensor projection $\mathbf{e}^n = \mathbf{e} \cdot \mathbf{n}$ into the first integral in Eq. (23), we can factor out $\mathbf{e}$ in front of the integral and get an integral that is fully determined by the strain tensor variation $\delta\mathbf{e}$ and thus, taken alone, represents a potential. As for the second integral, however, an analogous operation is impossible because $\partial\gamma^{\sigma}/\partial\gamma \neq \mathbf{n}$, in contrast to Eq. (24). Indeed, substituting the tensor projection of $\boldsymbol{\sigma}^{\mathbf{n}} = \boldsymbol{\sigma} \cdot \mathbf{n}$ does not yield an integral fully determined by the variation $\delta\mathbf{s}$ of the strain tensor that provides the kinematic constraint, and thus is not a total variation of a potential in terms of the macroscopic variables $\mathbf{e}$ and $\mathbf{s}$. To overcome this problem, recall the Legendre transformation which is, for instance, used to obtain the Gibbs free energy from the Helmholtz free energy. To this end, we rewrite Eq. (23) as follows:

$$\delta[\rho \boldsymbol{\mathcal{B}}(\mathbf{e}, \boldsymbol{\sigma})] = \int_{\Omega'} \mathbf{s}^e \cdot \left(\frac{\partial \mathbf{e}^n}{\partial \mathbf{e}} : \delta\mathbf{e} \right) d\Omega' - \int_{\Omega'} \gamma^{\sigma} \cdot \left(\frac{\partial \boldsymbol{\sigma}^n}{\partial \boldsymbol{\sigma}} : \delta\boldsymbol{\sigma} \right) d\Omega' \tag{25}$$

or

$$\boldsymbol{\sigma} : \delta\mathbf{e} - \boldsymbol{\gamma} : \delta\boldsymbol{\sigma} = \delta\mathbf{e} : \int_{\Omega'} \mathbf{s}^e \mathbf{n} d\Omega' - \delta\boldsymbol{\sigma} : \int_{\Omega'} \gamma^{\sigma} \cdot \mathbf{n} \, d\Omega' \tag{26}$$

in which $\partial\boldsymbol{\sigma}^n / \partial\boldsymbol{\sigma} = \mathbf{n}$ and

$$\rho \boldsymbol{\mathcal{B}}(\mathbf{e}, \boldsymbol{\sigma}) = \int \boldsymbol{\sigma} : d\mathbf{e} - \int \boldsymbol{\gamma} : d\boldsymbol{\sigma} = \rho \Psi_{\mathbf{e}} - \int_{\Omega'} \boldsymbol{\sigma}^n : \boldsymbol{\gamma}^{\sigma} d\Omega' \tag{27}$$

Now we denote

$$\delta(\rho \Psi_{\mathbf{e}}) = \int_{\Omega'} \mathbf{s}^e \cdot \delta\mathbf{e}^n d\Omega'$$

$$\delta(\rho \Upsilon_{\boldsymbol{\sigma}}) = \int_{\Omega'} \gamma^{\sigma} \cdot \delta\boldsymbol{\sigma}^n d\Omega'$$

$$\delta[\boldsymbol{\mathcal{B}}(\mathbf{e}, \boldsymbol{\sigma})] = \delta \ominus \mathbf{e} - \delta \mp \boldsymbol{\sigma} \tag{28}$$

All these expressions represent total variations, and so $\Psi_{\mathbf{e}}, \Upsilon_{\boldsymbol{\sigma}}$, and $\boldsymbol{\mathcal{B}}(\mathbf{e}, \boldsymbol{\sigma})$ represent thermodynamic potentials; $\Psi_{\mathbf{e}}$ and $\boldsymbol{\mathcal{B}}(\mathbf{e}, \boldsymbol{\sigma})$=potentials as functions of internal macroscopic variable $\mathbf{e}$ which is not directly measurable, even for homogeneous deformation. Only $\Upsilon_{\boldsymbol{\sigma}}$ is a potential as a function of a measurable continuum variable $\boldsymbol{\sigma}$; it represents specific Gibbs free energy associated with the statically constrained microplane system. The total potential (per unit volume) is

$$\boldsymbol{\mathcal{B}}(\mathbf{e}, \boldsymbol{\sigma}) = \Psi - \frac{1}{\rho} \int_{\Omega'} \boldsymbol{\sigma}^n \cdot \boldsymbol{\gamma}^{\sigma} d\Omega' = \Psi_{\mathbf{e}} - \Upsilon_{\boldsymbol{\sigma}} \tag{29}$$

It is a mixed potential (per unit volume) representing a superposition of specific Helmholtz and Gibbs free energies (Bažant 2002) for the isothermal material properties (for adiabatic material properties, this potential represents a mixture of specific total energy and enthalpy). The validity of this mixed potential is verified by the fact that the conditions of stationarity of this potential with respect to arbitrary variations $\delta\boldsymbol{\sigma}$ and $\delta\mathbf{e}$ yield, respectively, the expressions for $\boldsymbol{\gamma}$ and $\boldsymbol{\sigma}$ in terms of microplane stresses and strains, i.e., Eqs. (5) and (7). Integration of this potential over the structure volume and addition of external work yields a mixed potential of the structure–load system, which allows detecting bifurcation and deciding stability of the postbifurcation equilibrium paths [Bažant 1988; Bažant and Cedolin 1991, Eq. (10.2.15)].

The energy dissipation inequality, of course, cannot be checked from the present potential based on tangential stiffness. However, from the model coupling (visualized in Fig. 1 of Bažant and Caner 2005) it is physically clear that if the behavior on each microplane of a system, constrained either kinematically or statically, ensures non-negative energy dissipation, the dissipation inequality must be satisfied.

Closing

At this point, the constitutive model has been theoretically formulated. What remains are the computational aspects, particularly the computational algorithm and the calibration by test data. This is taken up in Part II of this study (Bažant and Caner 2005) which follows.

References

Barenblatt, G. I. (1959). "The formation of equilibrium cracks during brittle fracture. General ideas and hypothesis, axially symmetric cracks." *Prikl. Mat. Mekh.,* 23(3), 434–444.

Batdorf, S. B., and Budianski, B. (1949). "A mathematical theory of plasticity based on the concept of slip." *Technical Note No. 1871*, National Advisory Committee for Aeronautics, Washington, D.C.

Bažant, Z. P. (1984). "Microplane model for strain controlled inelastic behavior." *Mechanics of engineering materials*, C. S. Desai and R. H. Gallagher, eds., Chap. 3, Wiley, London, 45–59.

Bažant, Z. P. (1988). "Stable states and paths of structures with plasticity or damage." *J. Eng. Mech.,* 114(12), 2013–2034.

Bažant, Z. P. (2002). "Thermodynamic potential for microplane model M5 with kinematic and static constraints." *Progress Note*, Dept. of Civil Engineering, Northwestern Univ., Evanston, Ill.

Bažant, Z. P., Adley, M. D., Carol, I., Jirásek, M., Akers, S. A., Rohani, B., Cargile, J. D., and Caner, F. C. (2000b). "Large-strain generalization of microplane model for concrete and application." *J. Eng. Mech.,* 126(9), 971–980.

Bažant, Z. P., and Becq-Giraudon, E. (2002). "Statistical prediction of fracture parameters of concrete and implications for choice of testing standard." *Cem. Concr. Res.* 32(4), 529–556.

Bažant, Z. P., and Caner, F. C. (2005). "Microplane model M5 with kinematic and static constraints for concrete fracture and anelasticity. II: Computation." *J. Eng. Mech.,* 131(1), 41–47.

Bažant, Z. P., Caner, F. C., Adley, M. D., and Akers, S. A. (2000c). "Fracturing rate effect and creep in microplane model for dynamics." *J. Eng. Mech.,* 126(9), 962–970.

Bažant, Z. P., Caner, F. C., Carol, I., Adley, M. D., and Akers, S. A.

(2000a). "Microplane model M4 for concrete: I. Formulation with work-conjugate deviatoric stress." *J. Eng. Mech.*, 126(9), 944–953.

Bažant, Z. P., and Cedolin, L. (1991). *Stability of structures: elastic, inelastic, fracture and damage theories*, Oxford University Press, New York; and 2nd Ed. (2003), Dover, New York.

Bažant, Z. P., and Gambarova, P. (1984). "Crack shear in concrete: Crack band microplane model." *J. Struct. Eng.*, 110(9), 2015–2035.

Bažant, Z. P., and Oh, B.-H. (1983a). "Crack band theory for fracture of concrete." *Mater. Struct.*, 16, 155–177.

Bažant, Z. P., and Oh, B.-H. (1983b). "Microplane model for fracture analysis of concrete structures." *Proc., Symp. on the Interaction of Non-Nuclear Munitions with Structures*, United States Air Force Academy, Colorado Springs, Colo., 49–53.

Bažant, Z. P., and Oh, B.-H. (1985). "Microplane model for progressive fracture of concrete and rock." *J. Eng. Mech.*, 111(4), 559–582.

Bažant, Z. P., and Oh, B.-H. (1986). "Efficient numerical integration on the surface of a sphere." *Z. Angew. Math. Mech.*, 66(1), 37-49.

Bažant, Z. P., and Planas, J. (1998). *Fracture and size effect in concrete and other quasibrittle materials*, CRC, Boca Raton, Fla.

Bažant, Z. P., and Prat, P. C. (1988a). "Microplane model for brittle plastic material: I. Theory." *J. Eng. Mech.*, 114(10), 1672–1688.

Bažant, Z. P., and Prat, P. C. (1988b). "Microplane model for brittle plastic material: II. Verification." *J. Eng. Mech.*, 114(10), 1689–1699.

Bažant, Z. P., Şener, S., and Prat, P. C. (1988). "Size effect tests of torsional failure of plain and reinforced concrete beams." *Mater. Struct.*, 21, 425–430.

Bažant, Z. P., Xiang, Y., Adley, M. D., Prat, P. C., and Akers, S. A. (1996a). "Microplane model for concrete. II. Data delocalization and verification." *J. Eng. Mech.*, 122(3), 255–262.

Bažant, Z. P., Xiang, Y., and Prat, P. C. (1996b). "Microplane model for concrete. I. Stress–strain boundaries and finite strain." *J. Eng. Mech.*, 122(3), 245–254.

Bažant, Z. P., and Zi, G. (2003). "Microplane constitutive model for porous isotropic rock." *Int. J. Numer. Analyt. Meth. Geomech.*, 27, 25–47.

Brocca, M., and Bažant, Z. P. (2000). "Microplane constitutive model and metal plasticity." *Appl. Mech. Rev.*, 53(10), 265–281.

Brocca, M., and Bažant, Z. P. (2001a). "Microplane finite element analysis of tube-squash test of concrete with shear angles up to 70°." *Int. J. Numer. Methods Eng.*, 52, 1165–1188.

Brocca, M., and Bažant, Z. P. (2001b). "Size effect in concrete columns: Finite-element analysis with microplane model." *J. Struct. Eng.*, 127(12), 1382–1390.

Brocca, M., Bažant, Z. P., and Daniel, I. M. (2001). "Microplane model for stiff foams and finite element analysis of sandwich failure by core indentation." *Int. J. Solids Struct.*, 38, 8111–8132.

Bronkhorst, C. A., Kalindindi, S. R., and Anand, L. (1992). "Polycrystalline plasticity and the evolution of crystallographic texture in fcc metals." *Philos. Trans. R. Soc. London, Ser. A*, 341, 443–477.

Brown, G. M. (1970). "A self-consistent polycrystalline model for creep under combined stress states." *J. Mech. Phys. Solids*, 18, 367–382.

Budianski, B., and Wu, T. T. (1962). "Theoretical prediction of plastic strains of polycrystals." *Proc., 4th U.S. National Congress of Applied Mechanics*, ASME, New York, 1175–1185.

Butler, G. C., and McDowell, D. L. (1998). "Polycrystal constraint and grain subdivision." *Int. J. Plast.*, 14(8), 703–717.

Camacho, G. T., and Ortiz, M. (1996). "Computational modeling of impact damage in brittle materials." *Int. J. Solids Struct.*, 33(20–22), 2899–2938.

Caner, F. C., and Bažant, Z. P. (2000). "Microplane model M4 for concrete: II. Algorithm and Calibration." *J. Eng. Mech.*, 126(9), 954–961.

Caner, F. C., Bažant, Z. P., and Červenka, J. (2002). "Vertex effect in strain-softening concrete at rotating principal axes." *J. Eng. Mech.*, 128(1), 24–33.

Carol, I., and Bažant, Z. P. (1995). "New developments in microplane/multicrack models for concrete." *Proc., Fracture Mechanics of Concrete Structures (FraMCoS 2)*, F. H. Wittman, ed., Aedificatio, Freiburg, Germany, 841–856.

Carol, I., and Bažant, Z. P. (1997). "Damage and plasticity in microplane theory." *Int. J. Solids Struct.*, 34(29), 3807–3835.

Carol, I., Bažant, Z. P., and Prat, P. C. (1991). "Geometric damage tensor based on microplane model." *J. Eng. Mech.*, 117(10), 2429–2448.

Carol, I., Jirásek, M., and Bažant, Z. P. (2001). "New thermodynamically consistent approach to microplane theory. Part I. Free energy and consistent microplane stresses." *Int. J. Solids Struct.*, 38(17), 2921–2931.

Carol, I., Jirásek, M., and Bažant, Z. P. (2004). "A framework for microplane models at large strain, with application to hyperelasticity" *Int. J. Solids Struct.*, 41, 511-557.

Christensen, R. M. (1979). *Mechanics of composite materials*, Wiley, New York.

Guinea, G. V., Planas, J., and Elices, M. (1994). "A general bilinear fit for the softening curve of concrete." *Mater. Struct.*, 27, 99–105.

Hill, R., and Rice, J. R. (1972). "Constitutive analysis of elastic-plastic crystal at arbitrary strain." *J. Mech. Phys. Solids*, 20, 401–413.

Hillerborg, A. (1985). "The theoretical basis of method to determine the fracture energy G_f of concrete." *Mater. Struct.*, 18(106), 291–296.

Hillerborg, A., Modéer, M., and Petersson, P. E. (1976). "Analysis of crack formation and crack growth in concrete by means of fracture mechanics and finite elements." *Cem. Concr. Res.*, 6, 773–782.

Hughes, T. J. R. (1984). "Numerical implementation of constitutive models: Rate-independent deviatoric plasticity." *Theoretical formulation for large-scale computations of nonlinear material behavior*, S. Nemat-Nasser, R. J. Assaro, and G. A. Hegemier, eds., Martinus Nijhoff, Dordrecht, The Netherlands, 29–57.

Jirásek, M., and Bažant, Z. P. (2002). *Inelastic analysis of structures*, Wiley, London.

Krieg, R. D., and Key, S. W. (1976). "Implementation of time dependent plasticity theory into structural computer programs." *Constitutive equations in viscoplasticity: Computational and engineering aspects*, J. A. Stricklin and K. J. Saczalski, eds., Vol. AMD-20, ASME, New York, 125–138.

Krieg, R. D., and Krieg, D. B. (1977). "Accuracies of numerical solution methods for the elastic-perfectly plastic model." *J. Pressure Vessel Technol.*, 99(4), 510–515.

Lin, T. H., and Ito, M. (1965). "Theoretical plastic distortion of a polycrystalline aggregate under combined and reversed stresses." *J. Mech. Phys. Solids*, 13, 103–115.

Lin, T. H., and Ito, M. (1966). "Theoretical plastic stress-strain relationship of a polycrystal." *Int. J. Eng. Sci.*, 4, 543–561.

Pande, G. N., and Sharma, K. G. (1982). "Multilaminate model of clays—A numerical evaluation of the influence of rotation of the principal stress axis." *Rep.*, Dept. of Civil Engineering, Univ. College of Swansea, Swansea, U.K.

Pande, G. N., and Xiong, W. (1982). "An improved multi-laminate model of jointed rock masses." *Proc., Int. Symp. on Numerical Models in Geomechanics*, R. Dungar, G. N. Pande, and G. A. Studder, eds., (Zürich, Switzerland), Balkema, Rotterdam, The Netherlands, 218–226.

Petersson, P. E. (1981). "Crack growth and development of fracture zones in plain concrete and similar materials." *Rep. No. TVBM 1006*, Lund Institute of Technology, Lund, Sweden.

Reuss, A. (1929). "Berechnung der Fließgrenze von Mischkristallen auf Grund der Plastizitätsbedingung für Einkristalle." *Z. Angew. Math. Mech.*, 9, 49–58.

Rice, J. R. (1968). "Mathematical analysis in the mechanics of fracture." *Fracture—An advanced treatise*, H. Liebowitz, ed., Vol. 2, Academic, New York, 191–308.

Réunion Internationale des Laboratoires d'Essais et de Recherche sur les Matériaux (RILEM) Recommendation. (1985). "Determination of fracture energy of mortar and concrete by means of three-point bend tests of notched beams." *Mater. Struct.*, 18(106), 285-290.

Simo, J. C., and Hughes, T. J. R. (1998). *Computational plasticity*, Springer, New York.

Simo, J. C., and Taylor, R. L. (1985). "Consistent tangent operators for

rate independent elastoplasticity." *Comput. Methods Appl. Mech. Eng.*, 48, 101–119.
Stroud, A. H. (1971). *Approximate calculation of multiple integrals*, Prentice-Hall, Englewood Cliffs, N.J.
Taylor, G. I. (1938). "Plastic strain in metals." *J. Inst. Met.*, 62, 307–324.
Voigt, W. (1889). "Über die Beziehung zwischen den beiden Elastizitätskonstanten isotroper Körper." *Wied. Ann.*, 38, 573–587.
Wilkins, M. L. (1964). "Calculation of elastic-plastic flow." *Methods of computational physics*, Vol. 3, B. Alder et al., eds., Academic, New York.
Zienkiewicz, O. C., and Pande, G. N. (1977). "Time-dependent multilaminate model of rocks—A numerical study of deformation and failure of rock masses." *Int. J. Numer. Analyt. Meth. Geomech.*, 1, 219–247.

Microplane Model M5 with Kinematic and Static Constraints for Concrete Fracture and Anelasticity. II: Computation

Zdeněk P. Bažant, F.ASCE,[1] and Ferhun C. Caner[2]

Abstract: Following the formulation of the constitutive model in the preceding Part I in this issue, the present Part II addresses the problems of computational algorithm and convergence of iterations. Typical numerical responses are demonstrated and the parameters of the model are calibrated by test data from the literature.

DOI: 10.1061/(ASCE)0733-9399(2005)131:1(41)

CE Database subject headings: Concrete; Fracture; Inelastic action; Damage; Softening; Finite element method; Numerical models.

Introduction

After formulating the microplane constitutive model in the preceding Part I (Bažant and Caner 2005), we are now ready to introduce a localization limiter preventing spurious mesh sensitivity, develop the numerical algorithm, and investigate the conditions of convergence of iterations. Then we will demonstrate typical numerical simulations, compare the model to the characteristic test data from the literature, and calibrate the model parameters.

Adjustment of Postpeak Softening Based on Fracture Energy

To prevent postpeak strain softening from causing spurious mesh sensitivity in finite element analysis, one may apply the crack band model (Bažant and Oh 1983), in which the energy dissipation per unit volume is adjusted according to the ratio of the element size h to the characteristic crack bandwidth l (a material length), so as to achieve mesh-indendent energy dissipation per unit area of the crack plane.

Postpeak strain softening is known to engender spurious mesh sensitivity in finite element analysis (Bažant 1976), with the energy dissipation per unit area of failure surface depending on the chosen finite element size. There are two expedient ways to avoid it: (1) on the constitutive level, by applying the crack band model (Bažant and Oh 1983), in which the energy dissipation per unit volume is adjusted according to the ratio of the element size h to the characteristic crack bandwidth l (a material length); and (2) on the finite element level, by using a composite finite element in which a softening finite element is coupled in three dimensions with unloading finite elements without adjusting the microplane constitutive law (Bažant et al. 2002, 2001b). The former, named Model M4f and developed by Bažant et al. (2002), is simpler and has been adopted for the present numerical studies. It may be briefly described as follows.

Width l is the characteristic size of the representative volume (or characteristic length) of material for which the microplane constitutive model has been calibrated by tests (as described for M4 in Caner and Bažant 2000). The area W_f under the postpeak softening portion of each microplane stress–strain curve, multiplied by l, represents a contribution to the fracture energy of the material, which must be a constant in order to avoid spurious mesh sensitivity (Bažant and Oh 1983). If element size $h=l$ is chosen, the energy dissipation will be correct without any adjustment of microplane constitutive laws. However, an adjustment is needed when $h \neq l$ because the strain softening tends to localize into a band of a single element width.

Energy equivalence requires the adjustment to be such that $W_f^* h = W_f l$ or $W_f^* = W_f l/h$, where W_f^* is the area under the postpeak softening curve of each microplane stress–strain curve (Fig. 1). This may be achieved by a horizontal rescaling of all the softening boundaries, tensile as well as compressive, in the ratio $r = l/h$; see Fig. 1 where Point 2 represents the point at which the softening begins. Let Point P be any point on the softening Boundary Curve 23, and let U be a point at the same level (same stress) on the Unloading Line 10. The rescaling must be such that Point P moves to Point P' for which $\overline{UP'} = r\overline{UP}$. This represents a horizontal affinity transformation with respect to Axis 10, which transforms softening Boundary Curve 23 to a new softening Boundary Curve $2'3'$.

When the element is too large, ratio r could be so small that the transformed softening curve exhibits a snapback, i.e., the slope at some points changes from negative to positive. Since static finite element analysis cannot cope with snapback instability, elements that large cannot be allowed.

For mathematical implementation it is somewhat inconvenient that the axis of affinity is inclined. Since the inclination is very steep compared to the slope of the softening boundary, it makes little difference if the inclined affinity Axis 24 is replaced by the vertical affinity Axis 45 such that the area 23012 be equal to the

[1]McCormick School Professor and W. P. Murphy Professor of Civil Engineering and Materials Science, Northwestern Univ., 2145 Sheridan Rd., Tech A135, Evanston, IL 60208. E-mail z-bazant@northwestern.edu

[2]Ramón y Cajal Fellow, ETSECCPB-ETCG, Univ. Politecnica de Catalunya, Jordi Girona 1-3, Ed.D2 D.305, Barclona 08034, Spain E-mail: ferhun.caner@upc.es; formerly, Visiting Scholar, Northwestern Univ., 2145 Sheridan Rd., Evanston, IL 60208.

Note. Associate Editor: Franz-Josef Ulm. Discussion open until June 1, 2005. Separate discussions must be submitted for individual papers. To extend the closing date by one month, a written request must be filed with the ASCE Managing Editor. The manuscript for this paper was submitted for review and possible publication on January 27, 2003; approved on February 13, 2004. This paper is part of the ***Journal of Engineering Mechanics***, Vol. 131, No. 1, January 1, 2005. ©ASCE, ISSN 0733-9399/2005/1-41–47/$25.00.

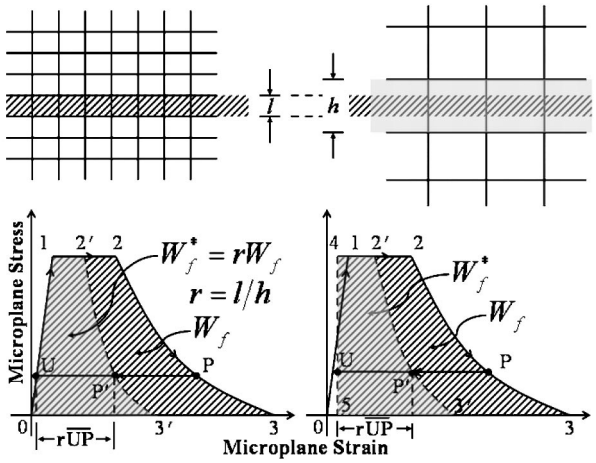

Fig. 1. (Top) Localized crack band; Adjustment of softening branches of microplane constitutive laws according to crack band model (proposed in Bažant et al. 2001); (bottom left) accurate method; (bottom right) simplified method

area 23542. Such rescaling is simpler and has been adopted for calculations.

Rescaling by this kind of affinity transformation is applied to tensile softening boundary of the statically constrained microplane system, which emulates the cohesive crack model for tension. It is also applied to each softening boundary in the kinematically constrained microplane system, i.e., to the softening positive and negative deviatoric boundaries, the tensile volumetric boundary, and the tensile normal boundary—the boundaries that control softening of the material in compression.

For a crack band running along the mesh lines of a rectangular or square mesh, h represents the width of the elements forming the crack band. For a crack band running through an irregular mesh, h cannot be defined exactly. However, it seems reasonable to simply assume that $h=4\times$ the ratio of the element area to the element perimeter, or $h=6\times$ the ratio of the element volume to its surface, in the case of two-or three-dimensional finite elements, respectively.

Numerical Comparisons with Test Data

Although the present Model M5 has been verified by comparisons with all the test data used in verifying Model M4 (Caner and Bažant 2000), comparisons of the tests with compressive or compressive-shear loading need not be reproduced here because they are identical or almost identical. The only significant change, and the advantage of this model, is found in tensile fracturing tests reaching into very large tensile strains.

Two typical data sets have been selected for fitting—those of Petersson (1981) for uniaxial tension, and of Bresler and Pister (1958) for combined shear and uniaxial compression (produced by torsional–axial loading). The latter data represent the compression shear envelope. Its points have been obtained by running simulations of response for different ratios of axial normal stress and shear stress, and collecting the peak points. Optimum fitting of both these data has succeeded to produce a satisfactory match; see Figs. 2 and 3.

In Fig. 4, the effect of the load step size on the uniaxial tension response is shown. It is demonstrated in this figure that the model response is accurate with strain increments on the order of 1

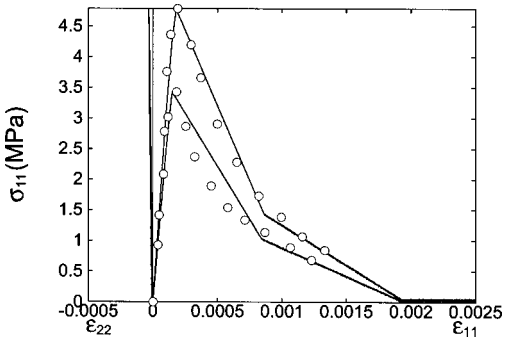

Fig. 2. Optimum fits of tensile softening test data of Petersson (1981), with corresponding lateral strain (data at bottom has compressive strength $f_c'=27$ MPa and other one $f_c'=41$ MPa); parameter values used in Model M5 are $k_1=0.000165$, $k_2=160$, $k_3=10$, $k_4=150$ with $\psi=0.3$, $\gamma_{N1}=0.005$, and $\gamma_{N2}=0.012$

$\times 10^{-5}$, just like its predecessors, despite the new algorithm which represents a radical improvement in the series of microplane models for concrete.

Convergence Criteria for Series Coupling Model with Softening

Since the formulation of a convergent iterative algorithm has been the crucial step making the present series coupling model possible, a deeper analysis of the covergence problem is in order. It will be instructive to consider first an algorithm which comes to mind more naturally (and has in fact been tried long ago, albeit with disappointing results). Then we will try another algorithm and show why, and when, it works.

Algorithm A. Predictor of Positive Stiffness

Consider a series coupling of two elements subjected to stress σ (Fig. 1). As the applied load is reduced, one element, with strain e, unloads with a positive tangent stiffness K, and the other, with

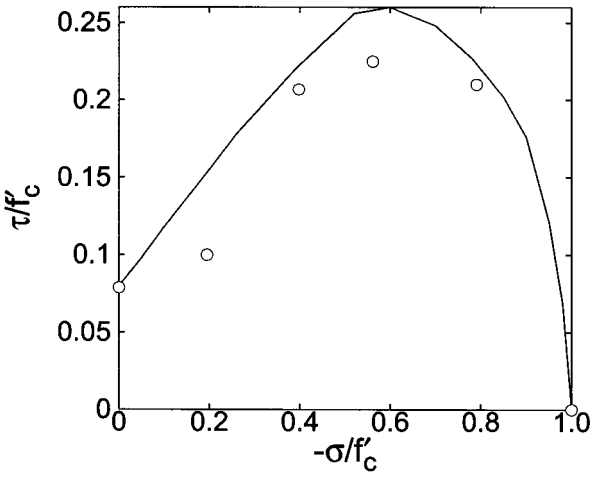

Fig. 3. Optimum fit of Bresler and Pister's (1958) test data for combined shear and uniaxial compression ($f_c'=68$ MPa); parameter values used in M5 are $k_1=0.0001$, $k_2=350$, $k_3=10$, $k_4=150$ with $\psi=0.3$, $\gamma_{N1}=0.005$, and $\gamma_{N2}=0.012$

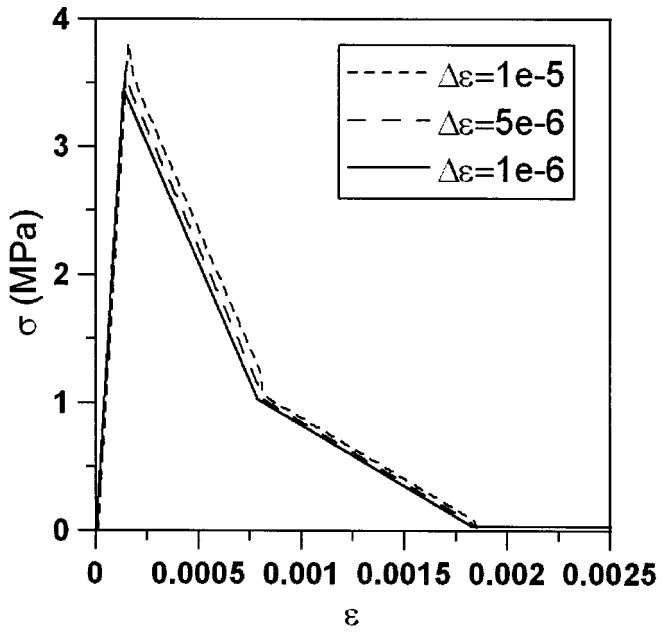

Fig. 4. Effect of loading step size in uniaxial tension response; the curve shown fits Petersson's data with $f_c'=27$ MPa already presented in Fig. 2

strain $\gamma=\epsilon-e$, expands with a negative tangent stiffness K_t (i.e., is softening). Scalars K and K_t, respectively, may be imagined as the overall tangential stiffnesses of the kinematically and statically constrained microplane systems for the actual direction of loading in the strain space.

In an iterative solution of the loading step, either K or K_t needs to be used as the predictor and the other as the corrector. In finite element programs for plasticity, the elastic deformation is used as the predictor, and the return to the current yield surface (i.e., the inelastic deformation) as the corrector. So, by analogy, it seems natural to use the positive (elastic) stiffness K as the predictor, and the inelastic stiffness K_t (a counterpart of the plastic hardening modulus) as the corrector. In this case, the algorithm of iterations (labeled by subscripts $i=1,2,3,\ldots$) for a given small step $\Delta\epsilon$ is as follows:

1. Denoting by subscript 0 the initial value at the beginning of the loading step, intialize either $\sigma_1=\sigma_0$ or $\sigma_1=\sigma_0+K\Delta e$, where Δe is the increment obtained in the previous loading step (the latter reduces the necessary number of iterations if γ varies smoothly).
2. Iteration loop, $n=1,2,3,\ldots N_{\text{it}}$; evaluate the predictor $\Delta\gamma=(\sigma_n-\sigma_0)/K_t$, and then the corrector $\sigma_{n+1}=\sigma_0+K(\epsilon-\epsilon_0-\Delta\gamma)$.
3. If the chosen tolerance is not met, reset $n\leftarrow n+1$, go to 2, and start a new iteration. Otherwise go to 1 and start the next loading step.

Overall, the algorithm leads to the following equation for the subsequent iterates σ_n:

$$\sigma_{n+1}+\frac{K}{K_t}\sigma_n=\left(1+\frac{K}{K_t}\right)\sigma_0+K(\epsilon-\epsilon_0) \tag{1}$$

This is a nonhomogeneous linear first-order difference equation with constant coefficients. It may be checked that its solution for initial value σ_1 is

$$\sigma_n=C\lambda^n+\sigma_\infty \tag{2}$$

with

$$\sigma_\infty=\sigma_0+\frac{\epsilon-\epsilon_0}{K^{-1}+K_t^{-1}},\qquad C=\frac{\sigma_1-\sigma_\infty}{\lambda} \tag{3}$$

Here λ, σ_∞, and C=constant during the iterations; λ is given by the characteristic equation $\lambda=-K/K_t$; and $\lambda>0$ for the postpeak. The iterations will converge if and only if $\lim_{n\to\infty}\lambda^n=0$, i.e., $|\lambda|<1$. So we conclude that an algorithm in which the positive stiffness is the predictor will converge if and only if

$$|K_t|>K$$

or

$$K_t<-K \tag{4}$$

Since the value of K_t may decrease continuously as ϵ increases during loading, we conclude that this iterative algorithm will inevitably diverge at least for the initial postpeak softening, if not always. This is unacceptable. Thus we arrive at a conclusion that might at first seem surprising: An algorithm analogous to the standard iterative algorithm with return to the yield surface, as used in incremental plastic finite element analysis, is impossible.

Algorithm B. Fracture-Based Predictor

Let us now explore an algorithm for which, in contrast to plastic finite element analysis, the negative stiffness K_t for the inelastic (fracturing) part γ of the total strain ϵ (Fig. 1) is used as the predictor, and K as the corrector. The algorithm for a given small loading step $\Delta\epsilon$ is as follows:

1. Either set $\Delta e_1=0$ or use for Δe_1 the value obtained in the preceding loading step (the latter shortens the iterations provided that e can be expected to evolve smoothly).
2. Iteration loop, $n=1,2,3,\ldots$; evaluate the predictor $\Delta\sigma=K_t(\Delta\epsilon-\Delta e_n)$ and then the corrector $e_{n+1}=\Delta\sigma_n/K$.
3. If the chosen tolerance is not met, reset $n\leftarrow n+1$, go to 2, and start a new iteration. Otherwise go to 1 and start the next loading step.

Overall, the algorithm leads to the following equation for the subsequent iterates Δe_n:

$$\Delta e_{n+1}+\frac{K_t}{K}\Delta e_n=\frac{K_t}{K}\Delta\epsilon \tag{5}$$

This is again a nonhomogeneous linear first-order difference equation with constant coefficients. It may be checked by substitution that its solution for initial value Δe_1 is

$$\Delta e_n=C\lambda^n+\Delta e_\infty \tag{6}$$

with

$$\Delta e_\infty=\frac{K}{K+K_t}\Delta\epsilon,\qquad C=\frac{\Delta e_1-\Delta e_\infty}{\lambda} \tag{7}$$

Here λ, Δe_∞, and C=constant during the iterations, and λ is given by the characteristic equation $K\lambda+K_t=0$, i.e., $\lambda=-K_t/K$. The it-

erations will converge if and only if $\lim_{n\to\infty}\lambda^n=0$, i.e., $|\lambda|<1$ or

$$|K_t|<K$$

or

$$K_t>-K \tag{8}$$

which is opposite to inequality (4). We thus conclude that, for postpeak softening, this iterative algorithm will work, unless the softening stiffness magnitude exceeds the elastic stiffness. The subsequent iterates form a geometric progression, and so the convergence is exponential.

Should we fear that inequality (8) might become violated for the normal behavior of concrete? To answer this question, consider the typical values $f_t'=3$ MPa, $G_f=30$ N/n (fracture energy corresponding to the initial tangent of the softening stress–separation curve of the cohesive crack model (Bažant 2002a,b), and average crack spacing $s=50$ mm. This furnishes for the average softening modulus for tensile cracking concrete the estimate $|K_t|=f_t'^2s/2G_f=7.5$ GPa, while the typical value of elastic modulus is $K\approx 26$ GPa, which is much higher than 7.5 GPa. Therefore, the limiting postpeak softening tangent modulus K_t for which the convergence of this algorithm would be lost will hardly ever be reached, for normal concrete and normal crack spacing. If inequality (8) is violated, one must question whether the considered crack spacing s is realistic. Reducing s causes a decrease of $|K_t|$ and thus helps convergence (just like reducing the finite element size in the crack band model).

Can Convergence Be Accelerated?

To accelerate convergence, one may try replacing the predictor in Step 2 of algorithm B, beginning with the third iteration ($n>2$), by $\Delta\sigma=K_t[\Delta\epsilon-\Delta e_n-\alpha(\Delta e_n-\Delta e_{n-1})]$, where α is an empirically chosen acceleration factor; $\alpha\in(0,1)$ might be expected to accelerate monotonic convergence, and $\alpha\in(-1,0)$ oscillatory convergence. The algorithm then leads (for $n>2$) to the equation

$$K\Delta e_{n+1}+K_t(1+\alpha)\Delta e_n-K_t\alpha\Delta e_{n-1}=K_t\Delta\epsilon \tag{9}$$

This is a nonhomogeneous linear second-order difference equation with constant coefficients. Solutions of its homogeneous part may be sought in the form $\Delta e_n=C\lambda^n$. Substituting this into Eq. (9), one gets the characteristic equation $K\lambda^2+(1+\alpha)K_t\lambda-\alpha K_t=0$, which has two roots

$$\left.\begin{matrix}\lambda_1\\ \lambda_2\end{matrix}\right\}=\frac{(1+\alpha)K_t}{2K}\left(-1\pm\sqrt{1+\frac{4\alpha K}{(1+\alpha)^2K_t}}\right) \tag{10}$$

The solution has the general form $\Delta e_{n+1}=C_1\lambda_1^n+C_2\lambda_2^n+\Delta e_\infty$, where Δe_∞ is the same as before and constants C_1 and C_2 must be solved from the initial Δe_n values for $n=1,2$. Now we observe that, if $a>0$, both roots are negative, but in that case a convergence acceleration would necessitate $\lambda<0$, a contradiction. If $\alpha<0$ (but not of a magnitude large enough to produce a complex root) λ_1 is positive, which calls for $\alpha>0$ but λ_2 is negative, which calls for $\alpha<0$, and so acceleration cannot be guaranteed. Therefore, a significant convergence acceleration with factor α seems, in general, unattainable.

There is, however, another way to accelerate convergence—use the Newton-Raphson algorithm, based on transential stiffness matrices of the statically and binematically constrained systems. It so happens that in the microplane model, they can be easily determined from microplane tangent stiffnesses.

Tensorial Analysis of Convergence of Algorithm B

Strictly speaking, the preceding analysis of convergence of algorithms A and B is valid only when Matrix K_t does not change from one iteration to the next. In general, it may change because the loading direction in the strain space need not be fixed but can rotate. Then the cnvergence must be analyzed tensorially. The generalized tensorial form of iterative algorithm B for a small loading step $\Delta\varepsilon$ reads, for $\alpha=0$, as follows:

1. Either set $\Delta\boldsymbol{e}_1=\mathbf{0}$ or use for $\Delta\boldsymbol{e}_1$ the tensorial increment obtained in the preceding loading step (the latter shortens the iterations provided that $\boldsymbol{e}$ can be expected to evolve smoothly).
2. Iteration loop, $n=1,2,3,\ldots$; Evaluate predictor $\Delta\boldsymbol{\sigma}=\boldsymbol{K}_t:[\Delta\boldsymbol{\varepsilon}-\Delta\boldsymbol{e}_n-\alpha(\Delta\boldsymbol{e}_n-\Delta\boldsymbol{e}_{n-1})]$, and then solve the corrector $\boldsymbol{e}_{n+1}$ from the equation $\Delta\boldsymbol{\sigma}_n=\boldsymbol{K}:\boldsymbol{e}_{n+1}$ (where the colon denotes a doubly contracted tensorial pruduct).
3. If the chosen tolerance is not met, reset $n\leftarrow n+1$, go to 2, and start a new iteration. Otherwise go to 1 and start the next loading step.

Overall, when all the vectors and second-order symmetiric tensors (denoted by italic bold letters and by $\boldsymbol{\epsilon}$) are replaced by 6×1 and 6×6 matrices (denoted by roman bold letters and by $\boldsymbol{\varepsilon}$), the algorithm leads to the following matrix equation for the subsequent iterates $\Delta\mathbf{e}_n$:

$$\Delta\mathbf{e}_{n+1}-\mathbf{A}\Delta\mathbf{e}_n=-\mathbf{A}\Delta\boldsymbol{\epsilon},\quad\text{with}\quad\mathbf{A}=-\mathbf{K}^{-1}\mathbf{K}_t \tag{11}$$

This is a nonhomogenous linear first-order matrix difference equation with constant matrix coefficients. It may be checked that its solution for initial value $\Delta\mathbf{e}_1$ is

$$\Delta\mathbf{e}_n=\mathbf{A}^n\mathbf{C}+\Delta\mathbf{e}_\infty \tag{12}$$

where

$$\Delta\mathbf{e}_\infty=-(\mathbf{I}-\mathbf{A})^{-1}\mathbf{A}\Delta\boldsymbol{\epsilon},\qquad\mathbf{C}=\mathbf{A}^{-1}(\Delta\mathbf{e}_1-\Delta\mathbf{e}_\infty) \tag{13}$$

in which $\mathbf{A}$, $\mathbf{C}$, and $\Delta\mathbf{e}_\infty$=constant square and column matrices during the iterations, and $\mathbf{I}$=unit 6×6 matrix.

To discuss convergence, consider that the coordinates are rotated (in a six-dimensional space), by rotation Matrix $\mathbf{R}$, into the principal directions of Matrix $\mathbf{K}$ (not to be confused with the principal directions of stress or strain tensor in three dimensions). We may also assume that the principal directions of Matrix $\mathbf{K_t}$ (in six dimensions) are the same. Then, in the principal coordinates, Matrix $\mathbf{A}$ becomes

$$\mathbf{A}'=\mathbf{R}^{\mathbf{T}}\mathbf{A}\mathbf{R}=\begin{bmatrix}K_1^{-1}&&&\\&K_2^{-1}&&\\&&\cdots&\\&&&K_6^{-1}\end{bmatrix}\begin{bmatrix}-K_{t1}&&&\\&-K_{t2}&&\\&&\cdots&\\&&&-K_{t6}\end{bmatrix}=\begin{bmatrix}\lambda_1&&&\\&\lambda_2&&\\&&\cdots&\\&&&\lambda_6\end{bmatrix} \tag{14}$$

where

$$\lambda_1=-K_1^{-1}K_{t1},\quad\lambda_2=-K_2^{-1}K_{t2},\ldots\lambda_6=-K_6^{-1}K_{t6} \tag{15}$$

Here $K_1,K_2,\ldots K_6$=eigenvalues of Matrix $\mathbf{K}$, and K_{t1}, $K_{t2},\ldots K_{t6}$=eigenvalues of Matrix $\mathbf{K}_t$. The iterations will converge if and only if $\lim_{n\to\infty}\mathbf{A}^n=\lim_{n\to\infty}\mathbf{A}'^n=\mathbf{0}$; i.e., all

$|\lambda_1|, |\lambda_2|, \ldots |\lambda_6|$ must be less than 1. This requires that

$$|K_{t1}| < K_1,$$
$$|K_{t2}| < K_2, \ldots |K_{t6}| < K_6 \tag{16}$$

Thus we have demonstrated tensorially that the iterative algorithm will converge if and only if each principal value of the tangent stiffness matrix for softening is smaller in magnitude than the corresponding principal value of the elastic stiffness matrix. The subsequent iterates form a matrix geometric progression.

Detailed Explicit Algorithm for M5

Finally, to permit unambiguous programming of the present model, the complete detailed algorithm for step-by-step loading will now be given. The strains and stresses at the beginning of each small loading step are known, and the material subroutine must deliver the stress tensor corresponding to a given strain tensor (and update the microplane history variables such as the maximum strain achieved so far). The stress tensor at various integration points is then used in numerical integration over the finite element to obtain the internal force vector of the element, and all these vectors from all the finite elements are then assembled to furnish the internal force vector of the structure.

The type of finite element program will decide when the microplane history variables should be updated. When the finite element program is explicit, these variables will be updated at the end of every time integration step. An implicit finite element program, on the other hand, will check whether convergence has been achieved, and only then it will update these variables. Once these microplane variables are updated, the stress tensor returned along with every other variable calculated in the finite element program using these stress components becomes validated.

The values of **n**, **m**, and l for each microplane are input in advance of finite element analysis and used to calculate tensors $N_{ij}=n_i n_j$, $M_{ij}=\text{sym}\ n_i m_j$, and $L_{ij}=\text{sym}\ n_i l_j$. These tensors are then stored to be used in structural analysis. The algorithm for the material subroutine is as follows:

1. The (macro)-strains ϵ_{ij} and their increments $\Delta\epsilon_{ij}$ are given. The microplane history stresses of the modified Model M4, s_N^0, s_L^0, and s_M^0, are stored for each microplane and s_V^0 is stored for all microplanes in the previously converged load step. Similarly, the microplane history strains of the statically constrained microplane model with cohesive law, γ_N^0, γ_N^0, and γ_M^0, are stored for each microplane in that step.
2. Set tolerance $=1\times10^{-12}$. Then reconstruct γ_{ij} and s_{ij} from the history variables via numerical integration of history variables:

$$\gamma_{ij} = \frac{3}{2\pi}\int_\Omega (\gamma_N^0 N_{ij} + \gamma_M^0 M_{ij} + \gamma_L^0 L_{ij}) d\Omega \tag{17}$$

$$s_{ij} = \frac{3}{2\pi}\int_\Omega \left[s_D^0\left(N_{ij} - \frac{\delta_{ij}}{3}\right) + s_M^0 M_{ij} + s_L^0 L_{ij}\right] d\Omega + s_V^0\delta_{ij} \tag{18}$$

3. Calculate $e_{ij}=\epsilon_{ij}-\gamma_{ij}$.
4. Compute the fracturing compliance, C_{ijkl}^f, and the current error in the additive split of increment of total strain, r_{ij}, that must be minimized as follows:
   (a) Using elastic stiffness Matrix K, compute the predictor $\Delta\sigma_{ij}=K_{ijkl}\Delta e_{kl}$;
   (b) Using static constraint, calculate the microplane stress increments: $\Delta\sigma_N=N_{ij}\Delta\sigma_{ij}$, $\Delta\sigma_M=M_{ij}\Delta\sigma_{ij}$, and $\Delta\sigma_L=L_{ij}\sigma_{ij}$;
   (c) The predicted total stress tensor now becomes $\sigma_{ij}=s_{ij}+\Delta\sigma_{ij}$ and, using the static constraint, the microplane stresses are calculated: $\sigma_N=N_{ij}\sigma_{ij}$, $\sigma_M=M_{ij}\sigma_{ij}$, and $\sigma_L=L_{ij}\sigma_{ij}$. Thereupon, the crack opening at all microplanes can be evaluated.
   i. Check whether $\gamma_N^0<1\times10^{-10}$; if true, set $\gamma_N^0=1\times10^{-10}$. Similarly, if $|\gamma_M^0|<1\times10^{-10}$ then set $\gamma_M^0=1\times10^{-10}\ \text{sgn}(\gamma_M^0)$, and if $|\gamma_L^0|=1\times10^{-10}$ then $\gamma_L^0=1\times10^{-10}\ \text{sgn}(\gamma_L^0)$.
   ii. Compute $\sigma=[\sigma_N^2+(\sigma_M^2+\sigma_L^2)\beta^{-2}]^{1/2}$. If $\sigma\neq0$ then $\Delta\sigma=[\Delta\sigma_N\sigma_N+(\Delta\sigma_M\sigma_M+\Delta\sigma_L\sigma_L)\beta^{-2}]/\sigma$, or else $\Delta\sigma=[\Delta\sigma_N^2+(\Delta\sigma_M^2+\Delta\sigma_L^2)\beta^{-2}]^{1/2}$, $\gamma^0=\{(\gamma_N^0)^2+[(\gamma_M^0)^2+(\gamma_L^0)^2]\beta^2\}^{1/2}$, and $\sigma^0=\sigma-\Delta\sigma$.
   iii. Set $Small=1\times10^{-2}f_t'$. For all microplanes, check if $\sigma+Small\leqslant0$, if true, set $\gamma_N=\gamma_M=\gamma_L=1\times10^{-10}$. Then calculate the elastic compliance $C=\min(\max(\gamma^0/\sigma^0,1\times10^{-5}),100)$. If $\sigma+Small>0$, calculate the cohesive law stress σ^b using Eqs. (16) of Part I at $\gamma=\gamma^0$. Also choose $0\leqslant k_u\leqslant1$.
   iv. Compute $\Delta\sigma^*=\sigma-\sigma^b$. If $\Delta\sigma^*>0$, first compute.

$$\gamma = \gamma^0 + \left(-\frac{\psi f_t'}{\gamma_{N2}-\gamma_{N1}}\right)\Delta\sigma^* \tag{19}$$

   and then calculate the fracturing compliances

$$C_N^f = \gamma/\sigma;$$
$$C_M^f = C_L^f = \beta^{-2}\gamma/\sigma \tag{20}$$

   v. If $\Delta\sigma^*\leqslant0$, calculate $\gamma=\gamma^0+k_u C\Delta\sigma$, Then compute $\gamma_N=\gamma\ \sigma_N/\sigma$, $\gamma_M=\gamma_{\sigma_M}/\sigma$, and $\gamma_L=\gamma\sigma_L/\sigma$; furthermore set the microplane fracturing compliances $C_N^f=C_M^f=C_L^f=Small$ for all microplanes.
   (d) Now calculate the predicted strain tensor increment by numerical integration:

$$\Delta_{\gamma_{ij}} = \frac{3}{2\pi}\int_\Omega (\gamma_N N_{ij} + \gamma_M M_{ij} + \gamma_L L_{ij}) d\Omega - \gamma_{ij} \tag{21}$$

   (e) Thus one arrives at the prediction of the current error in the additive split of increment of strain as $r_{ij}=-\Delta e_{ij}-\Delta\gamma_{ij}+\Delta\epsilon_{ij}$
   (f) Finally, the fracturing compliance tensor C_{ijkl}^f can be calculated as the integration of microplane compliances over the unit hemisphere

$$C_{ijkl}^f = \frac{3}{2\pi}\int_\Omega (C_N^f N_{ij}N_{kl} + C_M^f M_{ij}M_{kl} + C_L^f L_{ij}L_{kl}) d\Omega \tag{22}$$

5. It is convenient to adopt Voigt notation in what follows. In order to minimize the error r_i, $(i=1,2,\ldots6)$, its gradient is needed. It can be expressed in the Voigt notation as $G_{ij}=-C_{\text{in}}^f K_{nj}-\delta_{ij}(i,j,n=1,2,\ldots6)$ [see Eq. (13) in Part I], and it needs to be calculated only once when the equilibrium solution is achieved.
6. Set $\Delta e_i=0$, $(i=1,2,\ldots6)$ and implement a Newton–Raphson iterative algorithm in order to determine Δe_i that minimizes the error r_i by looping over the following steps:

(a) Calculate the error $r_i = r_i(\Delta e_i)$ for a given total strain increment $\Delta\epsilon_i$ using Steps 4a through 4b; (b) compute $\delta\Delta e_i = -G_{in}^{-1} r_n$ and replace Δe_i by $\Delta e_i + \delta\Delta e_i$; and (c) calculate the error magnitude as $\xi = (r_i r_i)^{1/2}$ and continue the loop until $\xi \leqslant$ tolerance. Typically tolerance $\approx 1 \times 10^{-3}$ for convergence at the initiation of the choesive fracture due to sudden onset of softening, and tolerance 1×10^{-12} at all other times.

7. Switching back to tensor notation, apply the kinematic constraint to get the microplane strain components $\Delta e_N = N_{ij}\Delta e_{ij}$, $\Delta e_V = \Delta e_{kk}/3$, $\Delta e_D = \Delta e_N - \Delta e_V$, $\Delta e_L = L_{ij}\Delta e_{ij}$, $\Delta e_M = M_{ij}\Delta e_{ij}$.
8. Check the loading criteria $s_V \Delta e_V > 0$, $s_D \Delta e_D > 0$, $s_T \Delta e_T > 0$ if loading, $s_V \Delta e_V \leqslant 0$, $s_D \Delta e_D \leqslant 0$, $s_T \Delta e_T \leqslant 0$ if unloading, and decide the value of the incremental elastic modulus on each microplane.
9. Compute $s_V^e = s_V^0 + E_V \Delta e_V$ and the boundary value $s_V^{b-} = F_V^-(-e_V)$; set

$$s_V^* = \max(s_V^{b-}, s_V^e) \tag{23}$$

10. Compute $s_D^e = s_D^0 + E_D \Delta e_D$ and the boundary values $s_D^{b-} = F_D^-(e_D)$ and also $s_D^{b+} = F_D^+(e_D)$; calculate

$$s_D = \min[\max(s_D^{b-}, s_D^e), s_D^{b+}] \tag{24}$$

11. For each microplane, compute $s_N = s_V^* + s_D$, and also s_N at the boundary as $s_N^b = F_N(e_N)$. But, to prevent violating the normal boundary, set

$$s_N = \min(s_N, s_N^b) \tag{25}$$

12. Recalculate s_V as the average of the microplane normal stress s_N over the surface of the unit hemisphere. But to prevent this value from exceeding the volumetric stress calculated in item 9 as s_V^*, set

$$s_V = \min\left(\int_\Omega s_N \, d\Omega/2\pi, \; s_V^* \right) \tag{26}$$

13. Recalculate $s_D = s_N - s_V$ for each microplane.
14. Calculate the shear stress at the boundary as $s_T^b = F_T(s_N)$ and the elastic shear stresses as $s_L^e = s_L^0 + E_T \Delta e_L$ and $s_M^e = s_M^0 + E_T \Delta e_M$; then, determine the shear stresses in $\boldsymbol{l}$ and $\boldsymbol{m}$ directions, respectively, as $s_L = \text{sgn}(s_L^e)\, \min(|s_T^b|, |s_L^e|)$ and $s_M = \text{sgn}(s_M^e)\, \min(|s_T^b|, |s_M^e|)$.
15. Compute the components of the (macro)-stress tensor by numerical integration over a unit hemisphere

$$s_{ij} = \frac{3}{2\pi} \int_\Omega \left[s_D \left(N_{ij} - \frac{\delta_{ij}}{3} \right) + s_M M_{ij} + s_L L_{ij} \right] d\Omega + s_V \delta_{ij} \tag{27}$$

16. Return stress tensor s_{ij} and history variables s_N, s_M, s_L, s_V, γ_N, γ_M, and γ_L to the finite element program.

It might seem that, as an alternative, one could calculate the error ξ in Step 6c in terms of Δs_{ij}, and if the tolerance were not satisfied, set $\Delta s_{ij}^{\text{pre}} = \Delta s_{ij}$, after which $\Delta s_{ij}^{\text{pre}}$ could be used in Step 4c. However, such an algorithm is found to diverge shortly after tensile softening begins.

Thanks to the inclusion of the Newton–Raphson algorithm in Step 6, strain increments as large as 2×10^{-5} gave accurate results. Initially, this algorithm was not included, and then strain increments as small as 10^{-8} had to be used to achieve good accuracy when steep tensile softening (or cracking) was in progress.

Conclusions

1. Microplane Model M5 achieves as realistic representation of progressive tensile cracking or cohesive fracture. It avoids stress locking and spurious excessive lateral contraction or expansion at very large postpeak tensile strains.
2. This improvement is achieved by a series coupling of two microplane systems: one constrained kinematically and the other statically. The latter simulates exclusively tensile cracking and fracture, while the former simulates all the nonlinear triaxial behavior in pure compression and compression with shear.
3. The coupling of two microplane systems in made possible by developing a new iterative algorithm which avoids solving the implicit nonlinear equations that relate the two microplane systems.
4. A special characteristic of this algorithm is that, in each loading step, the softening cohesive fracture properties of the statically constrained microplanes are used as the predictor and the hardening or properties of the kinematically microplanes are used as the corrector that returns the current state point to the stress–strain boundaries (softening yield limits). The roles of predictor and corrector are interchanged compared to the classical iterative returns mapping algorithms for hardening elasto–plastic behavior.
5. It is proven that the new iterative algorithm converges in a geometric progression, and the conditions of convergence are derived.
6. Except for a few minor differences, the constitutive properties on the kinematically constrained microplanes are the same as in the previous Model M4. In other words, except for tensile softening, the response is the same.
7. Further acceleration, with quadratic convergence, is achieved by using Newton-Raphson iterations to determine the strain subdivision between the two microplane systems. This is made possible by determining the tangential stiffnesses on that microplane level.
8. The softening cohesive fracture properties are related to the fracture energy and effective crack spacing in the same manner as in the preceding improved version M4f of microplane Model M4. The postpeak softening slope on the microplanes can be adjusted in the sense of the crack band model, to ensure the correct energy dissipation of localized fracture when the finite element size is varied.
9. The constitutive properties that differ from Model M4 are shown to allow good representation of test data for tensile softening of concrete and of the shear-compression failure envelope of concrete.
10. An incremental thermodynamic potential for the coupling of statically and kinematically constrained microplane models is formulated. If represents a combination of the Helmholtz and Gibbs free energy densities.

Acknowledgments

Parts I and II of this study were partially funded under Grant No. CMS-0732791 from the U.S. National Science Foundation and Grant No. DE-FG07-98ER45736 from the Department of Energy, made both to Northwestern University.

References

Bažant, Z. P. (1976), "Instability, ductility, and size effect in strain-softening concrete." *J. Eng. Mech. Div.,* 102(2), 331–344.

Bažant, Z. P. (2002a). *Scaling of structural strength*, Hermes Science, London.

Bažant, Z. P. (2002b). "Concrete fracture models: Testing and practice." *Eng. Fract. Mech.,* 69(2), 165-206.

Bažant, Z. P., and Caner, F. C. (2005). "Microplane model M5 with kinematic and static constraints for concrete fracture and anelasticity. I. Theory." *J. Eng. Mech.,* 131(1), 31–40.

Bažant, Z. P., Červenka, J., and Wierer, M. (2001). "Equivalent localization element for crack band model and as alternative to elements with embedded discontinuities." *Proc., 4th Int. Conf. Fracture Mechanics of Concrete Structures Paris*, R. de Borst et al., eds., Swets & Zeitlinger, A. A. Balkema, Lisse, The Netherlands, 765–772.

Bažant, Z. P., Červenka, J., and Wierer, M. (2001b). "Equivalent localization element for crack band approach to mesh-size sensitivity in microplane model." *Int. J. Numer. Methods Eng.* (in press).

Bažant, Z. P., and Oh, B.-H. (1983). "Crack band theory for fracture of concrete." *Mater. Struct.,* 16, 155–177.

Bažant, Z. P., Zi, G., and Jendele, L. (2002). "Softening adjustment of microplane model M4 based on fracture energy and crack band theory: Model M4f for Code ATENA." Private Communication to Dr. Jan Červenka, Červenka Company, Prague.

Bresler, B., and Pister, K. S. (1958). "Strength of concrete under combined stresses." *J. Am. Concr. Inst.,* 55(20), 321–345.

Caner, F. C., and Bažant, Z. P. (2000). "Microplane model M4 for concrete: II. Algorithm and calibration." *J. Eng. Mech.,* 126(9), 954–961.

Petersson, P. E. (1981). "Crack growth and development of fracture zones in plain concrete and similar materials." *Rep. No. TVBM 1006*, Lund Inst. of Technology, Lund, Sweden.